Reviewer #1

I still think you should have applied the retrieval to noisy data. I'm not asking for a perfect satellite simulation that replicates real viewing conditions and different spectral response function. Merely adding 3 % random perturbations to the observations underlying experiment F12 and F22 would be sufficient. There needs to be some evidence that the algorithm can deal with unavoidable noise to be of practical use. Such an analysis might also demonstrate that your predicted uncertainties are justified, improving the reader's confidence in your technique. (I'd actually prefer to see a thorough sensitivity study of bias as a function of the various parameters rather than the simple 1 - 3 % un- certainty you've added, but that can be in a third paper.)

A supplement has been added to the manuscript where experiment F22 is performed for AOT at $0.55\mu m$ varying from 0.05 to 0.8 with a 3% Gaussian noise.

I remain unhappy that a joint retrieval of aerosol and the surface is promised but only aerosol is discussed. There's a hint of a quite good surface retrieval at the end of Part 2 (and it's supplement). Yes, this paper is describing how the aerosol retrieval has been improved but your previous paper was from 2010. You can't have left the surface retrieval completely unaltered over almost a decade of research and, even if you did, I'd be rather surprised if all the changes you made to the aerosol scheme didn't impact the response of the surface scheme in some way. As you point out in your first sentence, the two are non-linearly coupled. Why decouple the papers when there's only one forward model?

Surface reflectance retrieval has already been discussed in a previous paper (Wagner et al., 2010) and is by far less challenging than aerosol retrieval as the magnitude of the signal due to the surface is much larger than the one from aerosols (see information content analysis in part 2). Surface retrieval is not addressed in this first part but in the second the second part. This has been clarified in the introduction where the following sentence has been added :

Practical aspects of the application of the CISAR algorithm for the retrieval of both surface and aerosol properties from actual satellite data are addressed in Luffarelli and Govaerts(2018) (hereafter referred to as Part II).

We do not understand the comment "Why decouple the papers when there's only one forward model?". Unfortunately we cannot answer it.

On L118, I don't think LUTs should be mentioned. The problems your describe aren't caused by the use of LUTs, but rather the use of LUTs that are either too coarse or are tabulated for insufficiently general variables. It is possible to build LUTs that have SSA and gas their axes. (As a side note, the GRASP algorithm of Dubovik's group was demonstrated on PARASOL data but can be, and has been, adapted to any sensor. As the information content decreases, the reliance on the prior increases.)

The reviewer is right. The outcome of a radiative transfer model can always be tabulated. In practice however the size of the LUT would become far too big for any practical use when the discretization step decreases or the number of variables increases. This is largely due to the radiative coupling between the atmosphere and the surface when anisotropic surface reflectance is accounted for.

You're entitled to use whatever terminology you like,but why not call the terms 'surface' and 'atmosphere' as you did in Govaerts et al. (2010)? 'Single' scattering could describe both single scattering by the surface and single scattering by an aerosol.

The manuscript always make clear whether single scattering is applied to atmospheric (aerosol) or surface properties. Unfortunately, we could not find a place in the manuscript where it is not the case and the comment does not refer to a specific paragraph or line number.

You missed my point about the beginning of your conclusions (now L425) for the example I gave. The third sentence of the conclusions implies you provided evidence of a fundamental flaw in retrievals that assume an aerosol type. You did no such thing and this statement should either be removed or edited to be accurately represented as an opinion.

We did not state that any types of aerosol retrieval based on aerosol classes is a fundamental flow. In Section 2, we explained that retrieval method based on OE required a continuous variations of the retrieved state variables which is not possible over land surface using only a limited number of aerosol classes when the radiative coupling between the surface and the aerosols. In the next comment, the reviewer wrote "Throughout the paper, you argue that assuming aerosol type is inconsistent with the assumptions of OE. I agree with that technical point" which is exactly what we claim here.

The third sentence of the conclusion reads now:

That analysis revealed that retrieval methods based on OE applied only to a limited number of aerosol classes as in Govaerts et al. (2010) represent a major drawback as it does not permit a continuous variation of the state variables in the solution space.

Apologies for my unclear remark on the title. Throughout the paper, you argue that assuming aerosol type is inconsistent with the assumptions of OE. I agree with that technical point. It is conceptually preferable to define state space in terms of the microphysical properties, as you have done. However, 'continuous variations of the state variables in solution space' will not convey that point to most readers as 'state variables' is not specific and all OE involves continuous variation of variables. Your enhancement is to select different variables to retrieve and constrain them through a choice of aerosol type (a.k.a. vertices).

We did not describe the aerosol state variables in terms of micro-physical properties. This is the approach of Dubovik's method. We only retrieve aerosol single scattering properties, not the microphysical properties such as index of refraction, radius distribution, sphericity, …

Your paper proposes something between Dubovik's direct retrieval of SSA- phase function and the assumed type of your previous algorithm. Aerosol types are still assumed (presumably to get around the highly non-Gaussian nature of the SSA-g prior distribution) but the retrieval may freely combine them to produce continuous variations in SSA and g . Hence, I would recommend a title along the lines of 'Retrieval of surface reflectance and aerosol microphysical properties through the mixture of representative aerosol types' but better worded. That emphasises the variation of aerosol mixture rather than the variables themselves.

As written in the previous comment, the CISAR algorithm does not retrieve aerosol micro-physical properties but the aerosol single scattering properties. It is therefore not appropriate to change the title stating that aerosol microphysical properties are retrieved. We do not follow the same approach as in GRASP to keep the number of state variables as low as possible.

To be pedantic, the techniques you critique are completely valid when evaluating only one type as they are effectively claiming to have perfect prior information about certain variables. That's obviously an inaccurate claim but it's statistically consistent. The inconsistency arises from the manner in which different types are combined.

I am not sure I fully understand this comment. An OE retrieval based on one aerosol class is indeed correct when forward simulations are performed using only that class. Anyway, any prior information should come with an uncertainty, which is not the case in Govaerts et al. (2010). That was the lesson learned from that paper that we address here.

I recommended deleting the sentence now starting on L354 as it is obvious that the uncertainty in SSA is larger than that in g since your retrieval could not vary g . As it stands, a reader unfamiliar with retrieval theory may not appreciate that your precise retrieval of g derives from having given it no other option (as the aerosol types provided demonstrate no variation in g .)

The sentence has been deleted.

Reading through Part 2, it became evident that Part 1 demonstrates retrievals using only one observation while Part 2 combines observations from 5-16 days. Why didn't you demonstrate the retrieval you actually intend to use? Presumably the additional data would improve the retrieval and provide better agreement? You spent several pages introducing the H matrices but it doesn't seem they played that much of a role in this paper. And, anticipating your response, a reader will be no more distracted by a few additional plots than they already are by Figs. 6-12. The retrievals could be plotted on the same axes, hopefully showing a reduction in uncertainty and bias as more overpasses are included.

Part 1 assumes instantaneous multi-angular observations. Technical aspects related to the generation of a multi-angular observation vector to characterize surface reflectance anisotropy have already been addressed in Govaerts et al. (2010) and Wagner et al. (2010). Part 1 describes a generic retrieval method which assumes that the observation vector is composed of multi-angular observations. Equations 11 to 20 are not specific or tuned for any particular instrument. The elaboration of the observation vector is described in detail in Part 2. The reduction of the uncertainty on the BHR retrieval as a result of the elaboration of the surface prior (as more overpasses are included) is shown in Part 2, Figure 20b. (Figure 12 in the revised manuscript)

If not doing that, I agree with the other reviewer's comments that Fig. 6-9 and 10-12 could be merged into single figures to facilitate comparison of the retrievals as a function of the vertices used.

Merging Fig 6-9 would give the following result:

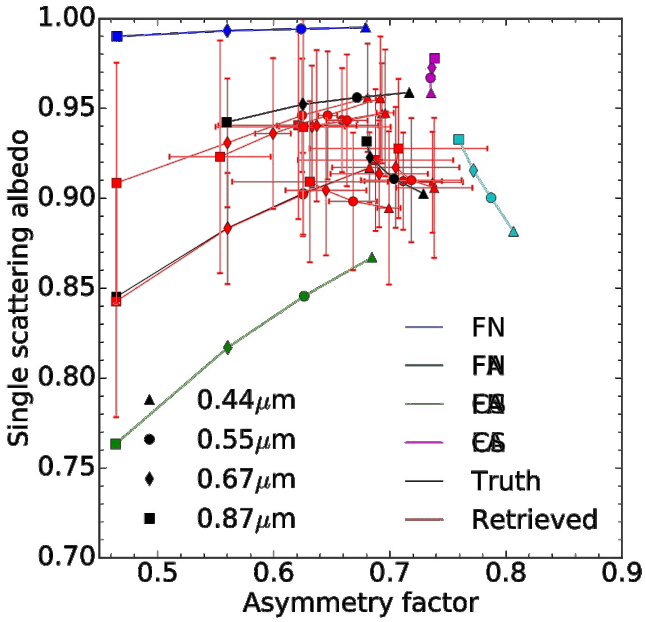

We found the resulting figure slightly too busy to be easily interpreted.

L18 I'd prefer to say "can be modelled as" rather than" Is equivalent to" as there are various possible models for this particular problem.

The sentence has been modified accordingly.

L309 Could you be more specific than'small'about this threshold?

It is a setup parameter that typically varies between 0.05 and 0.1.

L379 I disagree that ω0 is well retrieved; at 870 nm it's off by 0.03. The retrieved values are *consistent* with the truth, but so is half of the available range. If you insist that getting the range right is noteworthy, you need to provide an idea of how good these sorts of retrievals normally are and my memory is that AERONET is more accurate than 0.03 in these conditions. If I remember incorrectly, my apologies.

It is written reasonably well, it is retrieved within 3% of the true value at 870nm whereas g is off by about 20%. The CISAR algorithm does not pretend to compete with AERONET data.

L382 This uncertainty isn't underestimated—it is merely wrong. The retrieval wasn't given the ability to change *g* and so it considers it's retrieval to be very accurate.

Yes, the reviewer is correct. This experiment illustrates how the algorithm behave when it is the case.

In the conclusions, it would be more honest to mention the significant uncertainties in your retrievals at the end of L444 and to remove the word 'major' on L454.

The sentence L444 reads now:

These two classes have pretty different spectral behaviour in the [g,ω0] space and yet the CISAR algorithm is capable of retrieving the corresponding single scattering properties in both cases with estimated uncertainties of about 15%.

The word major on L454 has been kept as this new method addresses the two major weaknesses of Govaerts et al. (2010) discussed in Section 2.

All grammatical suggestions have been implemented.

Reviewer #2

- The entire draft fails to mention the presence of an accompanying Part II. With so many aspects not investigated in Part I, this seems a self-injury.

References to Part 2 has been added in Part I:

- In Sections 1, the following sentence has been added: *Practical aspects of the application of the CISAR algorithm for the retrieval of both surface and aerosol properties from actual satellite data are addressed in Luffarelli and Govaerts(2018) (hereafter referred to as Part II).*
- In the last sentence of Section 3*: In case of the processing of actual satellite data over a specific region or period, it is advised to calculate the isolines corresponding to that region of interest from AERONET observations and to adjust the position of the aerosol vertices accordingly as performed in Part II.*
- In Section 6.1, the following sentence has been added: *Part II explains how prior information on the surface parameters can be derived.*
- In the conclusion, the following sentence has been added at the end of the penultimate paragraph: *Part II addresses the CISAR performance when applied on actual satellite data*.

- The structure of the main body feels unbalanced. My impression is that the draft tries to tell the story of the different testing phases of the algorithm, from when its first lines were coded to its most recent version. I see no use for the description of the simplest experiments, which cannot be meaningfully applied to any practical retrieval. On the contrary, the paper fails to provide the reader with the most interesting piece of information, i.e. a solid understanding of how the vertices have to be chosen. If you determine that three vertices are enough, a more or less complete analysis of the performance has to be presented. Keeping a justified choice of the vertices as a baseline, performance variability should be discussed against a more complete set of aerosol distributions in the forward model.

It is not clear from which comment of Revision 2 reviewer #2 is referring to here. The manuscript presents a new method based on radiation transfer theory. Parts 1 illustrates how this new concept works with a set of simple experiments. The last paragraph of Section 3 has been added following revision 2 reviewer's comment. Two different method for the selection of the vertices are explained. The second method is used in Part 2 Section 3.2, where the vertices are located to encompass about 95% of AERONET observations.

- The value of 0.4 chosen as the optical thickness for all the simulations is just too specific and too high. Repeating the same analysis for -say- a set of taus in the range [0.05 - 1] would be the most natural choice and has the advantage to partially address the uncertainty of the method.

Following similar comment from Review #1 who was also asking for the impact of some random uncertainties in the simulations. A supplement has been generated showing the results of case F22 where AOT varies from 0.05 to 0.8 and a 3% Gaussian noise added to the simulated TOA BRF.

- With only one very specific example of RPV coefficients (moreover specified as a-priori knowledge), the title of manuscript sounds like an oversell. Does the method really perform well over different surfaces? How about over the ocean?

Refer to Part 2 for any type of surfaces. Over the ocean, surface reflectance is not retrieved but calculated with the Cox-Munk model, used taking surface wind speed from ECMWF.

- the term surface "anisotropy" deserves an explanation, as it is commonly referred to as an azimuthal asymmetry with respect to the principal plane, although both drafts seem to refer to just the angular distribution between 0 and 180 degrees

The term surface anisotropy has been replaced by surface reflectance anisotropy.

- Something has to be done with the complete lack of inclusion of noise in the simulated inversions. Either justifying moving its thorough assessment in Part II, or just including simple noise as previously suggested.

Reference to Part II has been has been clearly mentioned for this aspect. Refer also to the supplement which includes retrievals with a 3% random noise.

- Sec. 3 is important and needs to be reworked almost entirely. In particular, Fig. 2 needs to contain at least another wavelength (I suggest 0.87 um), or even better all of the 4 investigated bands. Why is the 1.60 um wavelength present when it is never used in the retrievals? Also, it must be clearly specified if the magnitude of the arrows is exactly the magnitude of the changes.

Wavelength 1.6 has been replaced by 0.8 in Fig. 2. The magnitude of the arrows is exactly the magnitude of the changes. It has been clarified in the text which reads now:

The magnitude of the red arrows illustrate the sensitivity to …

- The language is affected by many redundancies. Some concepts repeated over and over include "vertices delineate a subspace of the solution space where properties vary continuously". Long-winded, qualitative repetitions (see also the Conclusions) take the place of objective quantifications. They give the impressions that the main argument goes something like "Well, we're not sure when this algorithm works on real data, but at least it is different from Govaerts 2010 and hopefully it is better".

Language comments in the annotated pdf have been implemented. Please refer to Part 2 for the CISAR algorithm behaviour on real data. Part 2 is now explicitly referred to in the Conclusion.

If this algorithm has been operational in any form, it should be made clear not only in Part II, but also in Part I, unequivocally. For the paper's claims, case studies are not enough, although as they can be brought as testing examples.

Part 1 does not address any operational aspects related to the use of the CISAR algorithm. It is not the way the manuscript objective is formulated. Part 2 presents the outcome of two ESA founded studies aiming at apply the CISAR algorithm to SEVIRI and PROBA-V data. These two studies cover a wide range of different surface and aerosol types for two different observation conditions: polar and geostationary. Additionally, the CISAR algorithm is currently used for the processing of Sentinel-3A/SLSTR data in the framework of the ESA CIRCAS project (www.circas.eu). Finally, this algorithm is used within the H2020 FIDUCEO

project (www.fiduceo.eu) for the processing of the entire Meteosat First Generation archive. Publications with these latest results are in preparation.

Editor's comments

Following editor's suggestion, the following sentence has been added in the paragraph between Eq. 11 and 12.

The algorithm proposed by Dubovik et al. (2011) implements similar temporal and spectral smoothness constraints.

Manuscript prepared for Atmos. Meas. Tech.
with version 4.2 of the LaTeX class copernicus.cls.
Date: 26 May 2017

Joint retrieval of surface reflectance and aerosol properties with continuous variation of the state variables in the solution space: Part 1: theoretical concept

Yves Govaerts[1] and Marta Luffarelli[1]

[1]Rayference, Brussels, Belgium

Correspondence to: Yves Govaerts (yves.govaerts@rayference.eu)

Abstract. This paper presents a new algorithm for the joint retrieval of surface reflectance and aerosol properties with continuous variations of the state variables in the solution space. This algorithm, named CISAR (Combined Inversion of Surface and AeRosol), relies on a simple atmospheric vertical structure composed of two layers and an underlying surface. Surface anisotropic reflectance effects are taken into account and radiatively coupled with atmospheric scattering. For this purpose, a fast radiative transfer model has been explicitly developed, which includes acceleration techniques to solve the radiative transfer equation and to calculate the Jacobians. The inversion is performed within an optimal estimation framework including prior information on the state variable magnitude and regularization constraints on their spectral and temporal variability. In each processed wavelength, the algorithm retrieves the parameters of the surface reflectance model, the aerosol total column optical thickness and single scattering properties. The CISAR algorithm functioning is illustrated with a series of simple experiments.

1 Introduction

Radiative coupling between atmospheric scattering and surface reflectance processes prevents the use of linear relationships for the retrieval of aerosol properties over land surfaces. The discrimination between the contribution of the signal reflected by the surface and that scattered by aerosols represents one of the major issues when retrieving aerosol properties using spaceborne ~~imager~~ observations over land surfaces. Conceptually, this problem is equivalent to solving a radiative system composed of at least two layers, where the upper layers include aerosols and the bottom ones represent the soil/vegetation strata. The problem is further complicated by the intrinsic anisotropic radia-

tive behaviour of natural surfaces due to the mutual shadowing of the scattering elements, which is also affected by the amount of sky radiation (Govaerts et al., 2010, 2016). In most cases, an increase in aerosol concentration is responsible for an increase in the fraction of diffuse sky radiation which, in turn, smooths the effects of surface reflectance anisotropy. Though multi-spectral information is critical for the retrieval of aerosol properties, the spectral dimension alone does not allow full characterisation of the underlying surface reflectance which often offers a significant contribution to the total signal observed at the satellite level. In this regard, the additional information contained in multi-spectral and multi-angular observations through the joint retrieval of surface reflectance and aerosol properties has proven to be an efficient way to characterize aerosol properties over land surfaces.

Pinty et al. (2000a) pioneered the development of a retrieval method dedicated to the joint retrieval of surface reflectance and aerosol properties based on the inversion of a physically-based radiative model. This method has been subsequently improved to allow the processing of any geostationary satellites accounting for their actual radiometric performance (Govaerts and Lattanzio, 2007). This new versatile version of Pinty's algorithm has permitted the generation of a global surface albedo product from archived data acquired by operational geostationary satellites around the globe (Govaerts et al., 2008). These data included observations acquired by an old generation of radiometers with only one broad solar channel on-board the European Meteosat First Generation satellite, the US Geosynchronous Operational Environmental Satellite (GOES) and the Japanese Geostationary Meteorological Satellite (GMS). It is now routinely applied in the framework of the Sustained and COordinated Processing of Environmental satellite data for Climate Monitoring (SCOPE-CM) initiative for the generation of essential climate variables (Lattanzio et al., 2013). An improved version of this algorithm has been proposed by Govaerts et al. (2010) to take advantage of the multi-spectral capabilities of Meteosat Second Generation Spinning Enhanced Visible and Infrared Imager (MSG/SEVIRI) operated by EUMETSAT, and includes an Optimal Estimation (OE) inversion scheme using a minimization approach based on the Marquardt-Levenberg method (Marquardt, 1963).

The strengths and weaknesses of the algorithm proposed by Govaerts et al. (2010) are discussed in Section (2). In their proposed approach, the solutions of the Radiative Transfer Equation (RTE) are pre-calculated and stored in Look-Up Tables (LUTs) for a limited number of state variable values. Aerosol properties are limited to six different classes dominated either by fine or coarse particles. Two major drawbacks result from the use of pre-defined aerosol classes stored in pre-computed LUTs. Firstly, only a limited region of the solution space is sampled as a result of the reduced range of variability for state variables. For instance, in order to reduce the size of the LUTs, Pinty et al. (2000b) limit the maximum aerosol optical thickness to 1. Secondly, the solution space is not continuously sampled due to the use of pre-defined aerosol classes. Such an approach prevents an accurate retrieval of the solution at the expense of a very large number of classes. Dubovik et al. (2011) and

Diner et al. (2012), among others, demonstrated the advantages of a retrieval approach based on continuous variations of the aerosol properties as opposed to a LUT-based approach relying on a set of pre-defined aerosol classes. Even considering a large number of aerosol classes, LUT-based approaches under-perform methods with multi-variate continuity in the solution space (Kokhanovsky et al., 2010).

A new joint surface reflectance / aerosol properties retrieval approach is presented here that overcomes the limitations resulting from pre-computed RTE solutions stored in LUTs. This new method takes advantage of the lessons learned from past attempts to retrieve simultaneously surface reflectance and aerosol properties. The advantages of a continuous variation of the aerosol properties in the solution space against a LUT-based approach is discussed in Section (3). The proposed method expresses the scattering albedo and phase function values as a linear mixture of basic aerosol classes. The forward radiative transfer model that includes the Jacobians computation is described in Section (4). With the exception of gaseous transmittance, this model no longer relies on LUTs, and the RTE is explicitly solved. The inversion method is described in Section (5). Finally, the possibility to express aerosol single scattering properties as a linear combination is illustrated with simulated data representing various scenarios including small and large particles (6).

2 Lessons learned from previous approaches

Pinty et al. (2000a) proposed an algorithm for the joint retrieval of surface reflectance and aerosol properties to demonstrate the possibility of generating Essential Climate Variables (ECV) from data acquired by operational weather geostationary satellites. Due to limited operational computational resources available at that time in the EUMETSAT ground segment, where the data were processed, the development of this algorithm was subject to strong constraints. The RTE solutions were pre-computed and stored in LUTs with a very coarse resolution, limiting the maximum Aerosol Optical Thickness (AOT) to 1, which represented a severe limitation over the Sahara region where AOT values can easily exceed such limit. Furthermore, the radiative coupling between aerosol scattering and gaseous absorption was not taken into account. This algorithm, referred to as Geostationary Surface Albedo (GSA) has been subsequently modified by Govaerts and Lattanzio (2007) to include an estimation of the retrieval uncertainty. This updated version has permitted the generation of a global aerosol product derived from observations acquired by operational weather geostationary satellites (Govaerts et al., 2008). Since then, it is routinely applied in the framework of the SCOPE-CM initiative to generate a Climate Data Record (CDR) of surface albedo (Lattanzio et al., 2013).

The GSA algorithm has been further improved for the processing of SEVIRI data on-board MSG for the retrieval of the total column AOT from observations acquired in the VIS0.6, VIS0.8 and NIR1.6 spectral bands (Govaerts et al., 2010; Wagner et al., 2010). The method developed by these authors relies on an OE approach where surface reflectance and daily aerosol load are simultaneously

retrieved. The inversion is performed independently for each aerosol class and the one with the best fit is selected. A physically-based radiative transfer model accounting for non-Lambertian surface reflectance and its radiative coupling with atmospheric scattering is inverted against daily accumulated SEVIRI observations. However, this Land Daily Aerosol (LDA) algorithm suffers from two major limitations: (*i*) the use of pre-defined aerosol classes and, (*ii*) the algorithm delivers only one mean aerosol value per day when applied on MSG/SEVIRI data. This latter issue has been addressed by Luffarelli et al. (2016) who retrieve an aerosol optical thickness value for each SEVIRI observation. The former issue prevents a continuous variations of the state variables characterizing the aerosol single scattering properties as required by an OE approach (Rodgers, 2000). A consistent implementation of such approach is not straightforward since aerosol classes are defined as prior knowledge of the observed medium but no uncertainties are assigned to this information. Consequently, the estimated ~~retrieval~~ retrieval uncertainty is inconsistent as it does not account for the use of prior information and associated uncertainties.

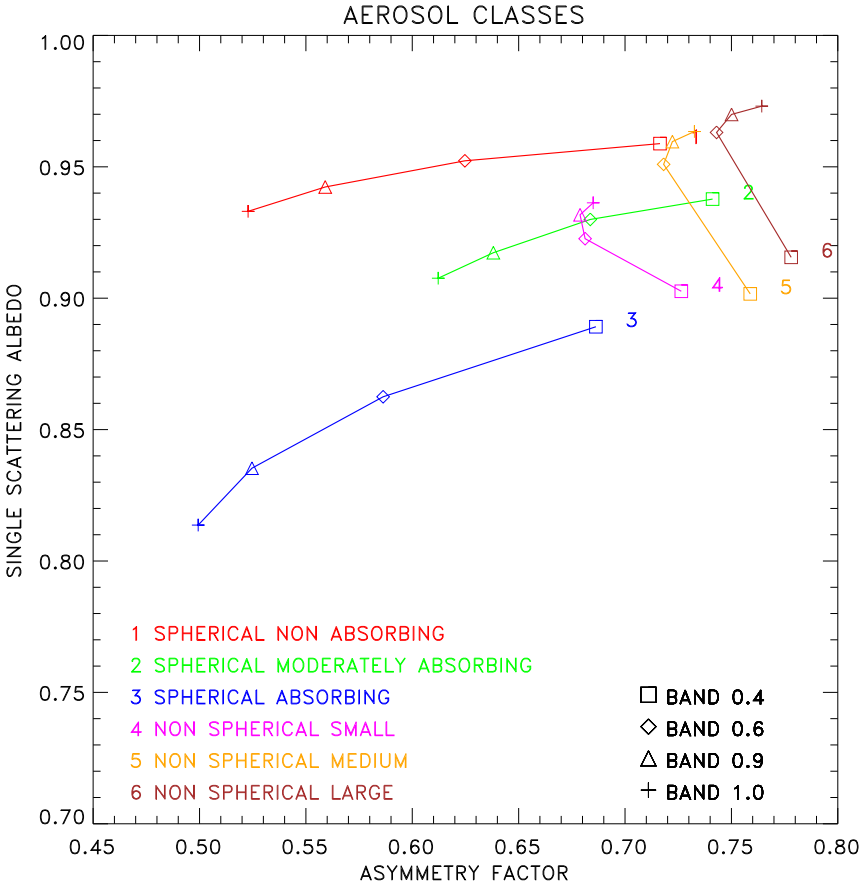

Fig. 1. Aerosol dual mode classes after Govaerts et al. (2010) in the $[g,\omega_0]$ space derived from the aggregation of aerosol single scattering properties retrieved from AERONET observations (Dubovik et al., 2006). Classes 1 to 3 are dominated by the fine mode and 4 to 6 by the coarse one.

Diner et al. (2012) demonstrated the advantages of a retrieval method based on continuous variations of aerosol single scattering properties in the solution space as opposed to a LUT-based approach derived for a limited number of pre-defined aerosol classes. Dubovik et al. (2011) proposed an original method for the retrieval of aerosol micro-physical properties which also does not necessitate the use of predefined aerosol classes. This method retrieved more than 100 state variables requiring therefore a considerable number of observations, such as those provided by multi-angular and -polarisation radiometers like Polarisation et Anisotropie des Réflectances Au SOmmet de l'Atmosphère (PARASOL) (Serene and Corcoral, 2006) or the future Multi-viewing Multi-channel Multi-polarization Imaging (3MI) instrument on-board EUMETSAT's Polar System Second Generation (Manolis et al., 2013). Instruments delivering such a large number of observations are rather scarce as most of the current or planned passive optical sensors do not offer instantaneous multi-angular observation capabilities nor information on polarization. The primary objective of this paper is to address the limitations resulting from conventional approaches based on LUTs and/or a limited number of pre-defined aerosol classes, proposing a method that can be applied to observations acquired by single or multi-view instruments.

3 Continuous variation of aerosol properties in the solution space

Aerosol single scattering properties include the single scattering albedo ω_0 and the phase function Φ in RTE. Govaerts et al. (2010) explained the benefits of representing pre-defined aerosol classes in a two-dimensional solution space composed of these aerosol single scattering properties. For the sake of clarity, they limited the phase function in that 2D space to the first term of the Legendre coefficients, *i.e.*, the asymmetry parameter g. However, one should keep in mind that the reasoning applied in this Section should be applied on the entire phase function Φ. These aerosol single scattering properties are themselves determined by aerosol micro-physical properties such as the particle size distribution, shape and their complex index of refraction. Within a retrieval approach based on aerosol classes, the objective is to provide the best possible sampling of the $[g,\omega_0]$ space such as in Govaerts et al. (2010). The inversion process proposed by these authors relies on a set of six classes which have been defined from AErosol RObotic NETwork (AERONET) data aggregation (Dubovik et al., 2006). These classes are supposed to provide the most likely sampling of the solution space but, since the scattering properties are not continuously varied, the inversion is typically repeated for each aerosol class and the one with the best fit is selected (Wagner et al., 2010).

A visual inspection of Fig. (1) after Govaerts et al. (2010) reveals that aerosol classes occupy different regions in the $[g,\omega_0]$ space according to the dominant particle size distribution, *i.e.*, fine or coarse. Within that space, an aerosol class is defined by the spectral behaviour of $\{g(\lambda),\omega_0(\lambda)\}$ pairs. The proposed fine mode classes vary mostly as a function ω_0 which is largely determined by the imaginary part of the refractive index n_i. Conversely, aerosol classes dominated by coarse

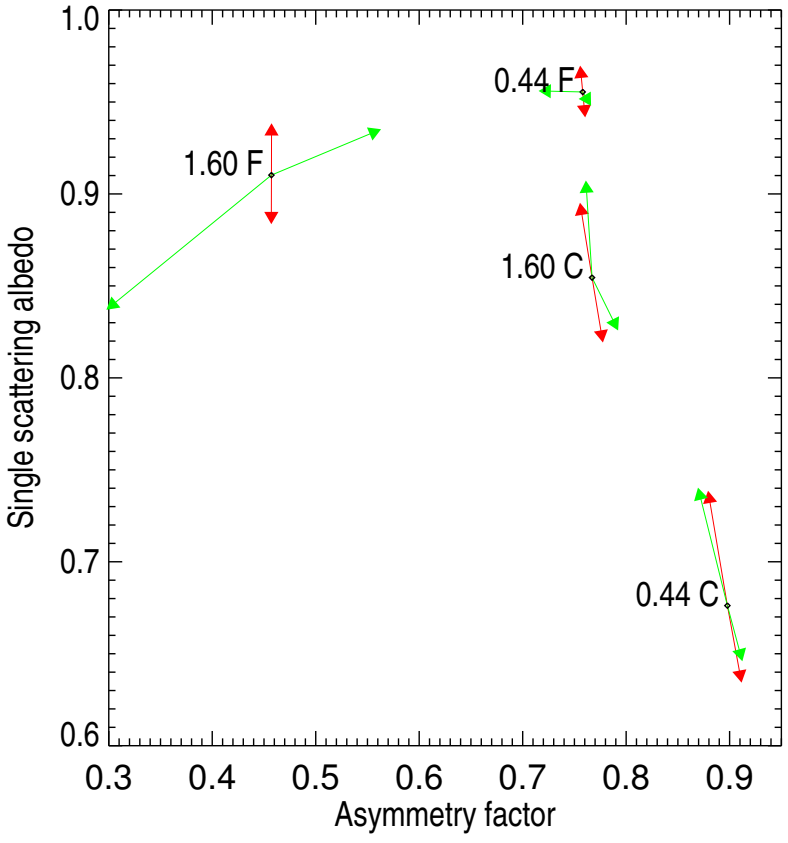

Fig. 2. Example of sensitivity of aerosol single scattering properties to particle median radius (green arrows) and imaginary part of the refractive index (red arrows) at 0.44μm and 1.60μm for fine mode F ($r_{mf} = 0.1\mu m$) and coarse mode C ($r_{mc} = 2.0\mu m$).

particles show little dependency on g and are therefore organised parallel to the ~~single scattering albedo~~ axis. The main parameter discriminating the~~se latter~~ classes is the median radius r_m, which essentially determines the asymmetry parameter value at a given wavelength~~ λ~~.

To illustrate the dependence of g and ω_0 on the median radius r_m and imaginary part of the refractive index n_i, fine and coarse mono-mode aerosol classes ~~have been~~ generated with $r_m = 0.15\mu m$ and 2.0μm respectively. The other micro-physical values ~~have been~~ fixed to $\sigma_r = 0.5\mu m$ $n_r = 1.42$ and $n_i = 0.008$ where σ_r is the radius standard deviation and n_r the real part of the refractive index. These values have been selected ~~on purpose~~ to ease the explanation of the aerosol classes organisation ~~on~~ Fig. (1). Black dots ~~on~~ Fig. (2) show the corresponding location ~~of the pair~~ of $\{g(\lambda),\omega_0(\lambda)\}$ ~~values~~ at 0.44μm and 1.60μm. Red arrows illustrate the sensitivity to a n_i change of ± 0.0025 and the green ones to a r_m change of $\pm 25\%$. For the fine mono-mode (F), changes in n_i essentially translate in displacement parallel to the ω_0 axis at short wavelengths while changes in

r_m result in changes parallel to the g axis. There is also a clear relationship between the particle size and g for that mode. A change in the particle size results in a change in g while ω_0 remains almost unchanged. The situation is quite different for the coarse mono-mode where changes in both n_i and r_m induce displacement parallel to the ω_0 axis with limited impact on g values. It should also be noted that the direction and magnitude of the changes depend on the wavelengths.

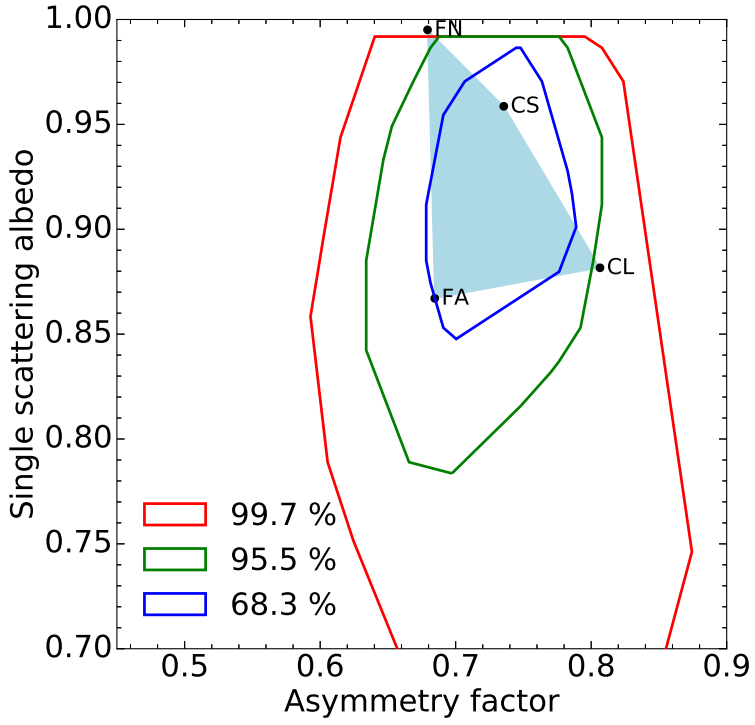

Fig. 3. Example of region (light blue area) in the $[g,\omega_0]$ solution space at 0.44μm defined by four aerosol vertices: single fine mode non-absorbing (FN), single fine mode absorbing (FA), coarse mode with small radius (CS) and coarse mode with large radius (CL). The isolines show the probability that the aerosol single scattering properties derived from Dubovik et al. (2006) fall within the delineated spaces.

The actual extent of possible solutions in the $[g,\omega_0]$ space for a given spectral band can be outlined by a series of vertices ~~characterizing aerosol single scattering properties~~. Following Fig. (2), these vertices are defined by an absorbing and a non-absorbing fine mono-mode classes with a small radius, labelled respectively FA and FN and by two coarse mono-modes with different radii, *i.e.*, large and small, labelled respectively CL and CS. ~~Such vertices define a polygon within the $[g,\omega$ solution space (Fig. 3).~~ The number of vertices can be adjusted according to the amount of spectral observations and expected type of aerosols. In Section (4), we will see how any pair of single scattering albedo and phase function values ~~in that space~~ can be expressed as a linear combination of the vertex properties.

The choice of the position of these vertices is critical as they should encompass most likely aerosol

single scattering properties that could be observed at a given time and location. ~~Different approaches could be used to define the position of these vertices~~. These positions could be derived from the analysis of typical aerosol single scattering properties available in databases such as Optical Properties of Aerosols and Clouds (OPAC) (Hess et al., 1998). Alternatively, it is also possible to follow a similar approach as the one proposed in Govaerts et al. (2010) who analysed the single scattering albedo and phase function values derived from AERONET observations acquired in a specific region of interest for a given period (Dubovik et al., 2006). ~~Fig. (3) shows an example of such type of analysis performed in the blue spectral region.~~ The red isoline on that Fig. delineates the area of the $[g,\omega_0]$ space where 99.7% of the aerosol single scattering properties derived by Dubovik et al. (2006) from AERONET observations are located. The green and blue lines show respectively the 95% and 68% probability regions. These values have been derived using all available Level 2 AERONET observations since 1993. Finally, the model proposed by Schuster et al. (2005) can be used to determine the spectral variations of the single scattering properties outside the spectral bands measured by AERONET. The present study relies on simulated data and the aerosol vertices have been positioned to sample the solution space in a realistic way. In case of the processing of actual satellite data over a specific region or period, it is advised to calculate the isolines corresponding to that region of interest from AERONET observations and to adjust the position of the aerosol vertices accordingly.

4 Forward Radiative Transfer Model

4.1 Overview

The forward model, named FASTRE, simulates the TOA Bidirectional Reflectance Factor (BRF) $y_m(\mathbf{x},\mathbf{b};\mathbf{m})$ as a function of independent parameters $\mathbf{m}$ defining the observation conditions and a series of state variables $\mathbf{x}$ describing the state of the atmosphere and underlying surface. Model parameters $\mathbf{b}$ represent variables such as total column water vapour that ~~influence the value of $y_m(\mathbf{x},\mathbf{b};\mathbf{m})$ but~~ cannot be retrieved ~~from the processed space-based observations~~ due to the lack of independent information. The independent parameters $\mathbf{m}$ include the illumination and viewing geometries (Ω_0,Ω_v) and the ~~spectral bands $\tilde{\lambda}$~~. The RTE is solved with the Matrix Operator Method (Fischer and Grassl, 1984) optimised by Liu and Ruprecht (1996) for a limited number of quadrature points.

The model simulates observations acquired within spectral bands $\tilde{\lambda}$ characterized by their spectral response. Gaseous transmittances in these bands are precomputed and stored in LUTs. ~~All other operations are calculated on the fly.~~ The model computes the contributions from single and multiple scattering separately, the latter being solved in Fourier space. In order to reduce the computation time, the forward model relies on the same atmospheric vertical structure as in Govaerts et al. (2010), *i.e.*, a three-level system containing two layers that are radiatively coupled (Fig. 4). The lowest level,

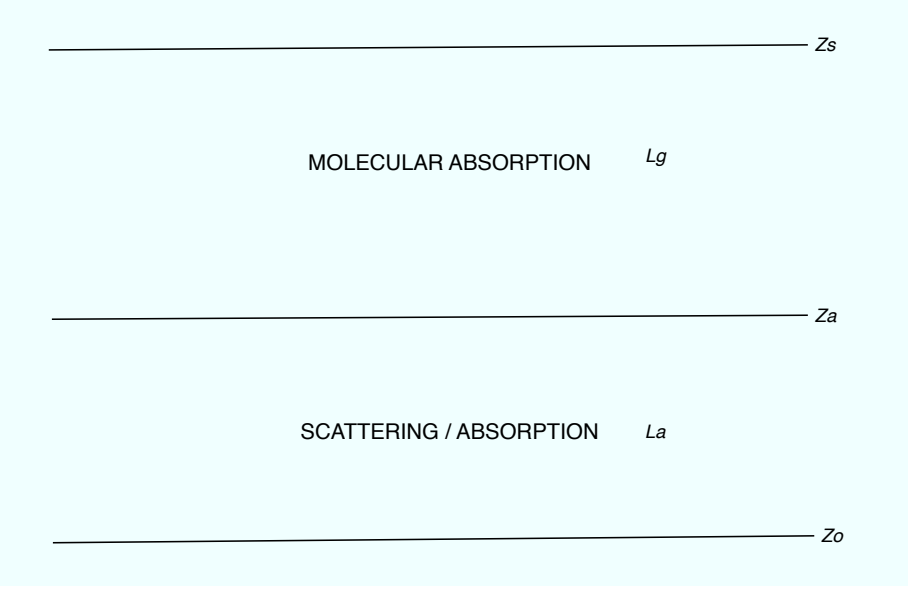

Fig. 4. Vertical structure of the FASTRE model. The surface is at level Z_0 and radiatively coupled with the lower layer L_a ~~running~~ from ~~level~~ Z_0 to Z_a. This layer includes scattering and absorption processes. The upper layer L_g runs from level Z_a to Z_s and only accounts for absorption processes.

Z_0, represents the surface. The lower layer L_a, ranging from levels Z_0 to Z_a, contains the aerosol particles. Molecular scattering and absorption are also taking place in that layer which is radiatively coupled with the surface for both the single and the multiple scattering. The upper layer L_g, ranging from Z_a to Z_s, is only subject to molecular absorption. ~~It is assumed that no scattering processes are taking place in that layer.~~

The surface reflectance $r_s(\mathbf{x_s},\mathbf{b};\mathbf{m})$ over land is represented by the so-called RPV (Rahman-Pinty-Verstraete) model ~~which has~~ four parameters $\mathbf{x_s} = \{\rho_0, k, \Theta, h\}$ that are all wavelength dependent (Rahman et al., 1993). ~~Each of these parameters control surface BRF differently~~. The ρ_0 parameter, included in the [0,1] interval, controls the mean amplitude of the BRF and strongly varies with wavelengths. The k parameter is the modified Minnaert's contribution that determines the bowl or bell shape of the BRF and ~~it~~ typically varies between 0 and 2. The asymmetry parameter of the Henyey-Greenstein phase function, Θ, varies between -1 and 1. The h parameter controls the amplitude of the hot-spot due to the "porosity" of the medium. This parameter ~~takes only positive values and~~ generally varies between 0 and 1. For the simulations over the ocean, the Cox-Munk model (Cox and Munk, 1954) is implemented (Vermote et al., 1997).

Aerosol single scattering properties in the layer L_a are represented by an external mixture of a series of predefined aerosol vertices as explained in Section (4.2). The L_g layer contains only absorbing gas not included in the scattering layer, such as high-altitude ozone, the part of the total column water vapour not included in layer L_a and few well-mixed gases.

The FASTRE model expresses the TOA BRF in a given spectral band $\tilde{\lambda}$ as a sum of the single $I_s^{\uparrow}$ and multiple $I_m^{\uparrow}$ scattering contributions as in

$$y_m(\mathbf{x},\mathbf{b};\mathbf{m}) = T_{L_g}(\mathbf{b};\mathbf{m})\,\frac{I_s^{\uparrow}(\mathbf{x},\mathbf{b};\mathbf{m}) + I_m^{\uparrow}(\mathbf{x},\mathbf{b};\mathbf{m})}{E_0^{\downarrow}(\mathbf{m})\mu_0} \tag{1}$$

where

. $I_s^{\uparrow}(\mathbf{x},\mathbf{b};\mathbf{m})$ is the upward radiance field at level Z_a due to the single scattering;

. $I_m^{\uparrow}(\mathbf{x},\mathbf{b};\mathbf{m})$ is the upward radiance field at level Z_a due to the multiple scattering;

. $T_{L_g}(\mathbf{b};\mathbf{m})$ denotes the total transmission factor in the L_g layer;

. $E_0^{\downarrow}(\mathbf{m})$ denotes the solar irradiance at level Z_s corrected for the Sun-Earth distance variations.

The single scattering contribution writes

$$I_s^{\uparrow}(\mathbf{x},\mathbf{b};\mathbf{m}) = \frac{E_0^{\downarrow}(\mathbf{m})\,\mu_0}{\pi}\exp\left(\frac{-\tau_{L_a}}{\mu_0}\right) r_s(\mathbf{x_s},\mathbf{b};\mathbf{m})\exp\left(\frac{-\tau_{L_a}}{\mu_v}\right) \tag{2}$$

where τ_{L_a} is the total optical thickness of layer L_a. μ_0 and μ_v are the cosine of the illumination and viewing zenith angles respectively.

The multiple scattering contribution $I_m^{\uparrow}(\mathbf{x},\mathbf{b};\mathbf{m})$ is solved in the Fourier space ~~in~~ all illumination and viewing directions of the quadrature directions N_θ for $2N_\theta - 1$ azimuthal directions. The contribution $I_m^{\uparrow}(\mathbf{x},\mathbf{b};\mathbf{m})$ in the direction (Ω_0,Ω_v) is interpolated from the surrounding quadrature directions. Finally, the Jacobian $\mathbf{k}_{x_i} = \frac{\partial y_m(\mathbf{x_i},\mathbf{b};\mathbf{m})}{\partial x_i}$ of $y_m(\mathbf{x},\mathbf{b};\mathbf{m})$ for parameter x_i are calculated as finite differences.

4.2 Scattering layer L_a properties

The layer L_a contains a set of mono-mode aerosol classes v characterized by their single scattering properties, *i.e.*, the single scattering albedo $\omega_{0,v}(\tilde{\lambda})$ and phase function $\Phi_v(\tilde{\lambda},\Omega_g)$ ~~in the spectral bands $\tilde{\lambda}$ at the phase angle Ω_g. These classes define the vertices encompassing the solution space, as illustrated in Fig. (3).~~ The different vertices ~~representing fine and coarse mode aerosols~~ are combined into this layer according to their respective optical thickness $\tau_v(\tilde{\lambda})$ with the total aerosol optical thickness $\tau_a(\tilde{\lambda})$ of the layer being equal to

$$\tau_a(\tilde{\lambda}) = \sum_v \tau_v(\tilde{\lambda}) \tag{3}$$

The phase function $\Phi_v(\tilde{\lambda},\Omega_g)$ ~~of an aerosol vertex~~ is characterized by a limited number N_κ of Legendre coefficients equal to $2N_\theta - 1$ ~~where N_θ is the number of quadrature points used to solve the multiple scattering integral~~. The choice of this number results from a trade-off between accuracy and ~~computer~~ time. When N_κ is too small, the last Legendre moment is often not equal to zero and the delta-M approximation is applied (Wiscombe, 1977). In ~~that~~ case, the α_d coefficient of the

delta-M approximation is equal to $\Phi_v(N_\kappa)$. The Legendre coefficients κ_j~~, after application of the delta-M approximation,~~ become

$$c_j = \frac{\kappa_j - \alpha_d}{1 - \alpha_d} \tag{4}$$

and the truncated phase function ~~denoted~~ Φ'_v. The corrected optical thickness $\tau'_v(\tilde{\lambda})$ and single scattering albedo $\omega'_{0,v}(\tilde{\lambda})$ of the corresponding aerosol class become

$$\tau'_v(\tilde{\lambda}) = (1 - \omega_{0,v}\alpha_d)\tau_v(\tilde{\lambda}) \tag{5}$$

and

$$\omega'_{0,v}(\tilde{\lambda}) = \frac{1 - \alpha_d}{1 - \omega_{0,v}\alpha_d}\omega_{0,v}(\tilde{\lambda})\,. \tag{6}$$

The layer total optical thickness, τ_{L_a}, is the sum of the gaseous, τ_g, the aerosol, τ'_a and the Rayleigh, τ_r, optical depth

$$\tau_{L_a}(\tilde{\lambda}) = \tau_g(\tilde{\lambda}) + \tau'_a(\tilde{\lambda}) + \tau_r(\tilde{\lambda}) \tag{7}$$

with $\tau'_a(\tilde{\lambda}) = \sum_v \tau'_v(\tilde{\lambda})$. The single scattering albedo of the scattering layer is equal to

$$\omega'_0(\tilde{\lambda}) = \frac{\sum_c \omega'_{0,v}(\tilde{\lambda})\,\tau'_v(\tilde{\lambda})}{\tau'_a(\tilde{\lambda})} \tag{8}$$

and the layer average phase function

$$\Phi'(\tilde{\lambda},\Omega_g) = \frac{\sum_c \Phi'_v(\tilde{\lambda},\Omega_g)\,\tau'_v(\tilde{\lambda})}{\tau'_a(\tilde{\lambda})}\,. \tag{9}$$

4.3 Gaseous layer properties

It is assumed that only molecular absorption ~~is taking~~ place in layer L_g. The height ~~of level~~ Z_a is used to partition the total column water vapour and ozone concentration in each layer assuming a US76 standard atmosphere vertical profile. This height is not retrieved and is therefore a model parameter of FASTRE which should be derived from some climatological values. T_{L_g} denotes the total transmission of that layer.

Table 1. Relative bias and root mean square error in percentage between FASTRE and the reference RTM in various spectral bands. Wavelengths are given in μm.

Spectral bands (μm)	0.44	0.55	0.67	0.87
Relative bias (%)	-1.1	-0.3	0.0	+0.3
Relative RMSE (%)	2.8	1.8	1.3	1.2

4.4 FASTRE model accuracy

The simple atmospheric vertical structure composed of two layers is the most important assumption of the FASTRE model. In order to evaluate the accuracy of FASTRE, a similar procedure as in Govaerts et al. (2010) has been applied. The outcome of FASTRE has been evaluated against a more elaborated 1D Radiative Transfer Model (RTM) (Govaerts, 2006) where the vertical structure of the atmosphere is explicitly taken into account for sun and viewing angles varying from 0 to 70°, for various types of aerosols, surface reflectance and total column water vapour values. The mean relative bias and relative Root Mean Square Error (RMSE) between the reference model and FASTRE have been estimated in the main spectral bands used for aerosol retrieval. The relative RMSE, R_r, is estimated ~~with~~

$$R_r = \sqrt{\frac{1}{N}\sum_{N}\left(\frac{y_m(\mathbf{x},\mathbf{b};\mathbf{m}) - y_r(\mathbf{x},\mathbf{b};\mathbf{r})}{y_r(\mathbf{x},\mathbf{b};\mathbf{r})}\right)^2} \tag{10}$$

where $y_r(\mathbf{x},\mathbf{b};\mathbf{m})$ is the TOA BRF calculated with the reference model. In this paper, the FASTRE model solves the RTE using 16 quadrature points N_θ which provides a good compromise between speed and accuracy. Results are shown ~~on~~ Table ~~(1)~~. ~~As can be seen, the~~ relative RMSE between FASTRE and the reference model is typically in the range of 1% – 3%. A similar comparison has been performed against actual PROBA-V observations (Luffarelli et al., 2017). These comparisons show a ~~root mean square error between simulated and actual observations~~ in the range 0.024–0.038.

5 Inversion process

5.1 Overview

Surface reflectance characterisation requires multi-angular observations $\mathbf{y}_{\Omega\tilde{\Lambda}}$, the acquisition of which can take between several minutes, as is the case for the Multi-angle Imaging SpectroRadiometer (MISR) instrument, and several days, as is the case for the Ocean and Land Colour Instrument (OLCI) on-board Sentinel-3 or the Moderate Resolution Imaging Spectroradiometer (MODIS). In the former case, data are often assumed being acquired almost instantaneously, *i.e.*, with the atmospheric properties remaining unchanged during the acquisition time. Such situation considerably reduces the calculation time required to solve the RTE, as the multiple scattering term $I_m^{\uparrow}(\mathbf{x},\mathbf{b};\mathbf{m})$ needs to be estimated only once per spectral band. In the latter case, atmospheric properties cannot be assumed to be invariant and the multiple scattering contribution needs to be solved for each observation. When geostationary observations are processed, the accumulation period is often reduced to one day, and the assumption that the atmosphere does not change can be converted into an equivalent radiometric uncertainty (Govaerts et al., 2010). Strictly speaking, it should be assumed that atmospheric properties have changed when the accumulation time exceeds several minutes (Luf-

farelli et al., 2016), ~~which increases the number of retrieved state variables to taken into account and therefore the processing time.~~

The retrieved state variables in each spectral band $\widetilde{\lambda}$ are composed of the $\mathbf{x_s}$ parameters characterising the state of the surface and the set of aerosol optical thicknesses τ_v for the aerosol vertices that are mixed in layer L_a. Prior information consists of the expected values $\mathbf{x_b}$ of the state variables $\mathbf{x}$ characterising the surface and the atmosphere on one side, and regularization of the spectral and/or temporal variability of τ_v on the other side. Uncertainty matrices $\mathbf{S}_x$ are assigned to this prior information. Finally, uncertainties in the measurements $\mathbf{S}_y$ are assumed to be normally distributed with zero mean. The inversion process of the FASTRE model will be herein referred to as Combined Inversion of Surface and AeRosol (CISAR) algorithm.

5.2 Cost function

The fundamental principle of Optimal Estimation (OE) is to maximise the probability $P = P(\mathbf{x}|\mathbf{y}_{\Omega\widetilde{\Lambda}},\mathbf{x_b},\mathbf{b})$ with respect to the values of the state vector $\mathbf{x}$, conditional to the value of the measurements and any prior information. The conditional probability takes on the quadratic form (Rodgers, 2000; Dubovik et al., 2011):

$$\begin{aligned} P(\mathbf{x}) \propto & \exp\left[-\left(y_m(\mathbf{x},\mathbf{b};\mathbf{m})-\mathbf{y}_{\Omega\tilde{\Lambda}}\right)^T \mathbf{S}_y^{-1}\left(y_m(\mathbf{x},\mathbf{b};\mathbf{m})-\mathbf{y}_{\Omega\tilde{\Lambda}}\right)\right] \\ & \exp\left[-\left(\mathbf{x}-\mathbf{x}_b\right)^T \mathbf{S}_x^{-1}\left(\mathbf{x}-\mathbf{x}_b\right)\right] \\ & \exp\left[-\mathbf{x}^T \mathbf{H}_a^T \mathbf{S}_a^{-1} \mathbf{H}_a \mathbf{x}\right] \\ & \exp\left[-\mathbf{x}^T \mathbf{H}_l^T \mathbf{S}_l^{-1} \mathbf{H}_l \mathbf{x}\right] \end{aligned} \tag{11}$$

where the first two terms represent weighted deviations from measurements and the prior state parameters, respectively, the third the AOT temporal smoothness constraints and the fourth the AOT spectral constraint, with respective uncertainty matrices $\mathbf{S}_a$ and $\mathbf{S}_l$. The two matrices $\mathbf{H}_a$ and $\mathbf{H}_l$, representing respectively the temporal and spectral constraints, can be written as block diagonal matrices

$$\mathbf{H} = \begin{pmatrix} \mathbf{H}^{\rho_0} & \mathbf{0} & \mathbf{0} & \mathbf{0} & \mathbf{0} \\ \mathbf{0} & \mathbf{H}^{k} & \mathbf{0} & \mathbf{0} & \mathbf{0} \\ \mathbf{0} & \mathbf{0} & \mathbf{H}^{\theta} & \mathbf{0} & \mathbf{0} \\ \mathbf{0} & \mathbf{0} & \mathbf{0} & \mathbf{H}^{\rho_c} & \mathbf{0} \\ \mathbf{0} & \mathbf{0} & \mathbf{0} & \mathbf{0} & \mathbf{H}^{\tau} \end{pmatrix} \tag{12}$$

where the four blocks $\mathbf{H}^{\rho_0}$, $\mathbf{H}^{k}$, $\mathbf{H}^{\theta}$ and $\mathbf{H}^{\rho_c}$ express the spectral constraints between the surface parameters. Their values are set to zero when these constraints are not active. The submatrix $\mathbf{H}_a^{\tau}$ can also be written using blocks $\mathbf{H}_{a;\tilde{\lambda},v}^{\tau}$ along the diagonal. For a given spectral band $\tilde{\lambda}$ and aerosol

vertex v, the block $\mathbf{H}^{\tau}_{a;\tilde{\lambda},v}$ is defined as follows

$$\mathbf{H}^{\tau}_{a;\tilde{\lambda},v}\,\boldsymbol{\tau}_{\tilde{\lambda},v} = \begin{pmatrix} 1 & -1 & 0 & \dots & \dots \\ 0 & 1 & -1 & 0 & \dots \\ \dots & \dots & \dots & \dots & \dots \\ \dots & \dots & \dots & 1 & -1 \\ \dots & \dots & \dots & \dots & 0 \end{pmatrix} \begin{pmatrix} \tau_{\tilde{\lambda},v,1} \\ \tau_{\tilde{\lambda},v,2} \\ \vdots \\ \tau_{\tilde{\lambda},v,N_t-1} \\ \tau_{\tilde{\lambda},v,1,N_t} \end{pmatrix} \tag{13}$$

In the same way, the submatrix $\mathbf{H}^{\tau}_{l}$ can be written using blocks $\mathbf{H}^{\tau}_{l;v,t}$. For a given aerosol vertex v and time t, the block $\mathbf{H}^{\tau}_{l;v,t}$ is defined as follows

$$\mathbf{H}^{\tau}_{l;v,t}\,\boldsymbol{\tau}_{v,t} = \begin{pmatrix} 0 & 0 & 0 & \dots & 0 \\ -\frac{\epsilon_2}{\epsilon_1} & 1 & 0 & \dots & 0 \\ 0 & -\frac{\epsilon_3}{\epsilon_2} & 1 & \dots & 0 \\ \dots & \dots & \dots & \ddots & 0 \\ \dots & \dots & \dots & -\frac{\epsilon_{N_\lambda}}{\epsilon_{N_\lambda-1}} & 1 \end{pmatrix} \begin{pmatrix} \tau_{1,v,t} \\ \tau_{2,v,t} \\ \tau_{3,v,t} \\ \vdots \\ \tau_{N_{\tilde{\lambda}},v,t} \end{pmatrix} \tag{14}$$

where the ϵ_l represents the uncertainties associated with the AOT spectral constraints of the individual vertex v bounding the solution space. The spectral variations of τ_v between band $\tilde{\lambda}_l$ and $\tilde{\lambda}_{l+1}$ ~~writes~~

$$\frac{\tau_{\tilde{\lambda}_l,v}}{\tau_{\tilde{\lambda}_{l+1},v}} = \frac{e_{\tilde{\lambda}_l}}{e_{\tilde{\lambda}_{l+1}}} \tag{15}$$

where $e_{\tilde{\lambda}_l}$ the extinction coefficient in band $\tilde{\lambda}_l$.

Maximising the probability function in Equation (11) is equivalent to minimising the negative logarithm

$$J(\mathbf{x}) = J_y(\mathbf{x}) + J_x(\mathbf{x}) + J_a(\mathbf{x}) + J_l(\mathbf{x}) \tag{16}$$

with

$$J_y(\mathbf{x}) = \left(y_m(\mathbf{x},\mathbf{b},\Omega) - \mathbf{y}_{\Omega\tilde{\Lambda}}\right) \mathbf{S}_y^{-1} \left(y_m(\mathbf{x},\mathbf{b},\Omega) - \mathbf{y}_{\Omega\tilde{\Lambda}}\right)^T \tag{17}$$

$$J_x(\mathbf{x}) = \left(\mathbf{x} - \mathbf{x}_b\right) \mathbf{S}_x^{-1} \left(\mathbf{x} - \mathbf{x}_b\right)^T \tag{18}$$

$$J_a(\mathbf{x}) = \mathbf{x}^T\, \mathbf{H}_a^T\, \mathbf{S}_a^{-1}\, \mathbf{H}_a\, \mathbf{x} \tag{19}$$

$$J_l(\mathbf{x}) = \mathbf{x}^T\, \mathbf{H}_l^T\, \mathbf{S}_l^{-1}\, \mathbf{H}_l\, \mathbf{x} \tag{20}$$

Notice that the cost function J is minimized with respect to the state variable $\mathbf{x}$, so that the derivative of J is independent of the model parameters $\mathbf{b}$ ~~which therefore cannot be part of the solution~~. The need for angular sampling to document the surface anisotropy leads to an unbalanced size of n_x and n_y with $n_y > n_x$ where n_y and n_x represents the number of observations and state variables respectively. According to Dubovik et al. (2006), these additional observations should improve the retrieval as, from a statistical point of view, repeating the same observation implies that the variance ~~of repeated similar observations~~ should decrease. Accordingly, the magnitude of the

elements of the covariance matrix should decrease as $1/\sqrt{n_y}$. Thus, repeating similar observations results in some enhancements of retrieval accuracy which should be proportional to the ratio n_y/n_x. Hence, the cost function which is actually minimized is $J_s(\mathbf{x}) = J_y(\mathbf{x}) + n_y/n_x\,(J_x(\mathbf{x}) + J_a(\mathbf{x}) + J_l(\mathbf{x}))$.

5.3 Retrieval uncertainty estimation

The retrieval uncertainty is based on the OE theory, assuming a linear behaviour of $y_m(\mathbf{x},\mathbf{b};\mathbf{m})$ in the vicinity of the solution $\hat{\mathbf{x}}$. Under this condition, the retrieval uncertainty $\sigma_{\hat{\mathbf{x}}}$ is determined by the shape of $J(\mathbf{x})$ at $\hat{\mathbf{x}}$

$$\sigma^2_{\hat{\mathbf{x}}} = \left(\frac{\partial^2 J_s(\mathbf{x})}{\partial \mathbf{x}^2}\right)^{-1} = \left(\mathbf{K}_x^T\,\mathbf{S}_y^{-1}\,\mathbf{K}_x + \mathbf{S}_x^{-1} + \mathbf{H}_a^T\,\mathbf{S}_a^{-1}\,\mathbf{H}_a + \mathbf{H}_l^T\,\mathbf{S}_l^{-1}\,\mathbf{H}_l\right)^{-1} \tag{21}$$

where $\mathbf{K}_x$ is Jacobian matrix of $y_m(\mathbf{x},\mathbf{b};\mathbf{m})$ calculated in $\hat{\mathbf{x}}$. Combining Equations (21) and (8), the uncertainty in the retrieval of ω_0 in band $\tilde{\lambda}$ writes

$$\sigma^2_{\hat{\omega}_0}(\tilde{\lambda}) = \sum_v \left(\frac{\omega_{0,v}(\tilde{\lambda}) - \omega_0(\tilde{\lambda})}{\tau_a(\tilde{\lambda})}\right)^2 \sigma^2_{\hat{\tau}_v}(\tilde{\lambda}) \tag{22}$$

A similar equation can be derived for the estimation of σ^2_g.

5.4 Acceleration methods

The minimization of Equation (16) relies on an iterative approach with $y_m(\mathbf{x},\mathbf{b};\mathbf{m})$ and the associated Jacobians $\mathbf{K}_x$ being estimated at each iteration. In order to reduce the calculation time dedicated to the estimation of $y_m(\mathbf{x},\mathbf{b};\mathbf{m})$ and $\mathbf{K}_x$, a series of methods have been implemented. All quantities that do not explicitly depend on the state variables, such as the observation conditions $\mathbf{m}$, model parameters $\mathbf{b}$, quadrature point weight, *etc*, are computed only once prior to the optimization.

When solving the RTE, the estimation of the multiple scattering term is by far the most time-consuming step. Hence, during the iterative optimisation process, when the change $\Delta\tau_a(\tilde{\lambda})$ ~~of $\tau_a(\tilde{\lambda})$~~ between iteration j and $j+1$ is small, the multiple scattering contribution at iteration $j+1$ is estimated with

$$I^{\uparrow}_m(\tau_a(j+1,\tilde{\lambda}),\mathbf{b};\mathbf{m}) = I^{\uparrow}_m(\tau_a(j,\tilde{\lambda}),\mathbf{b};\mathbf{m}) + \frac{\partial I^{\uparrow}_m(\tau_a(j,\tilde{\lambda}),\mathbf{b};\mathbf{m})}{\partial \tau_a}\,\Delta\tau_a(\tilde{\lambda}) \tag{23}$$

This approximation is not used twice consecutively to avoid inaccurate results, and the single scattering contribution is always explicitly estimated.

6 Algorithm performance evaluation

6.1 Experimental setup

A ~~simple~~ experimental setup based on simulated data has been defined to ~~illustrate~~ the ~~behaviour~~ of the CISAR algorithm ~~as a function of the delineated solution space~~. More specifically, its capability

Table 2. List of aerosol properties used for the simulations. The parameters r_{mf} and r_{mc} are the median fine and coarse mode radii expressed in μm. Their respective standard deviations are $\sigma_{r_{mf}}$ and $\sigma_{r_{mc}}$. The parameters n_r and n_i are the real and imaginary part of the refractive index in the indicated bands. N_f and N_c are the fine and coarse mode particle concentration in number of particles per cm^3.

Centre band in μm			0.44	0.55	0.67	0.87		
Type	r_{mf}	r_{mc}	n_i	n_r	n_r	n_r	N_f	N_c
F0	0.08	-	1.3958	1.3932	1.3909	1.3879	-	-
F1	0.10	0.93	1.4189	1.4269	1.4357	1.4417	9.587	0.002
F2	0.08	0.77	1.4985	1.5201	1.5436	1.5417	8.975	0.024
	$\sigma_{r_{mf}}$	$\sigma_{r_{mc}}$	n_i	n_i	n_i	n_i		
F0	0.45	-	0.0123	0.0123	0.0122	0.0121	-	-
F1	0.43	0.62	0.0057	0.0055	0.0053	0.0051		
F2	0.50	0.62	0.0054	0.0047	0.0040	0.0036		

to continuously sample the $[g,\omega_0]$ solution space is examined in detail. For the sake of simplicity, a noise-free multi-angular observation vector $\mathbf{y}_{\Omega\tilde{\Lambda}}$, where Ω expresses the illumination and viewing geometries, is assumed to be acquired instantaneously in the principal plane and in the spectral bands listed in Table (1). ~~An~~ uncertainty of 3% is assumed ~~in matrix~~ $\mathbf{S}_y$. In this ideal configuration, the Sun Zenith Angle (SZA) is set to 30°. It is also assumed that the surface parameters are known a priori with zero bias and an uncertainty of 0.03 for each RPV parameter, though these parameters are allowed to vary. Such assumption can be justified applying the method and associated results described in Wagner et al. (2010). No prior information is assumed for the aerosol optical thickness, *i.e.*, the prior uncertainty is set to very large values. Only regularization on the spectral variations of τ_a is applied.

Table 3. Micro-physical parameter values for the four FA, FN, CS, CL vertices in the selected spectral bands. Radius are given in μm

Centre band in μm			0.44	0.55	0.67	0.87	0.44	0.55	0.67	0.87
Type	r_m	σ_{r_m}	n_r	n_r	n_r	n_r	n_i	n_i	n_i	n_i
FN	0.08	0.45	1.3958	1.3932	1.3909	1.3879	0.0006	0.0006	0.0006	0.0006
FA	0.08	0.45	1.3958	1.3932	1.3909	1.3879	0.0207	0.0207	0.0207	0.0205
CS	0.30	0.55	1.4889	1.4878	1.4845	1.4763	0.0029	0.0029	0.0029	0.0029
CL	1.00	0.55	1.4889	1.4878	1.4845	1.4763	0.0029	0.0029	0.0029	0.0029

The CISAR algorithm performance evaluation is based on a series of experiments corresponding to different selections of aerosol properties, both for the forward simulation of the observations and their inversion. Three different aerosol models are used in the forward simulations: F0 which only contains small particles, F1 which contains a dual-mode particle size distribution dominated

by small particles, and F2 composed of a dual-mode distribution dominated by the coarse particles. Table (2) contains the values of the size distribution and refractive indices of these aerosol classes. Corresponding values for the four FA, FN, CL, CS vertices enclosing the solution space as illustrated in Fig. (3) are given in Table (3). When the observations simulated with aerosol types F0, F1 or F2 are inverted, the list of vertices actually used depends on the type of experiments indicated in Table (4). ~~The objective of these experiments is to illustrate the impact of the selected solution space on the retrieved aerosol properties.~~ For all these scenarios, an AOT of 0.4 at 0.55μm is assumed.

Table 4. List of experiments the name of which is provided in the first column. The active vertices in each experiments are indicated with the $\times$ symbol. The last column indicates the name of the aerosol model used to simulate the observations.

Exp.	Active vertices				Forward type
	FA	FN	CS	CL	
F00	$\times$	$\times$			F0
F10	$\times$	$\times$			F1
F11	$\times$	$\times$	$\times$		F1
F12	$\times$	$\times$		$\times$	F1
F13	$\times$	$\times$	$\times$	$\times$	F1
F21	$\times$	$\times$	$\times$		F2
F22	$\times$	$\times$		$\times$	F2
F23	$\times$	$\times$	$\times$	$\times$	F2

Table 5. Values of the surface RPV parameters ~~as~~ used ~~in the experiments for the~~ prior information. ~~Wavelengths are given in μm.~~

Wavelength	ρ_0	k	Θ	ρ_c
0.44	0.025	0.666	-0.150	0.125
0.55	0.047	0.657	-0.114	0.023
0.67	0.056	0.710	-0.096	0.025
0.87	0.238	0.706	-0.019	0.030

Values used for the RPV parameters in the four selected bands are indicated in Table (5). They correspond to typical BRF values that would be observed over a vegetated surface with a leaf area index value of 3 and a bright underling soil.

The primary objective of these experiments is to illustrate the behaviour of the proposed algorithm as a function of the selected vertices. It is therefore not intended to demonstrate that the algorithm can work in all possible conditions. Examples of retrieval against actual satellite observations can be found in Luffarelli et al. (2016).

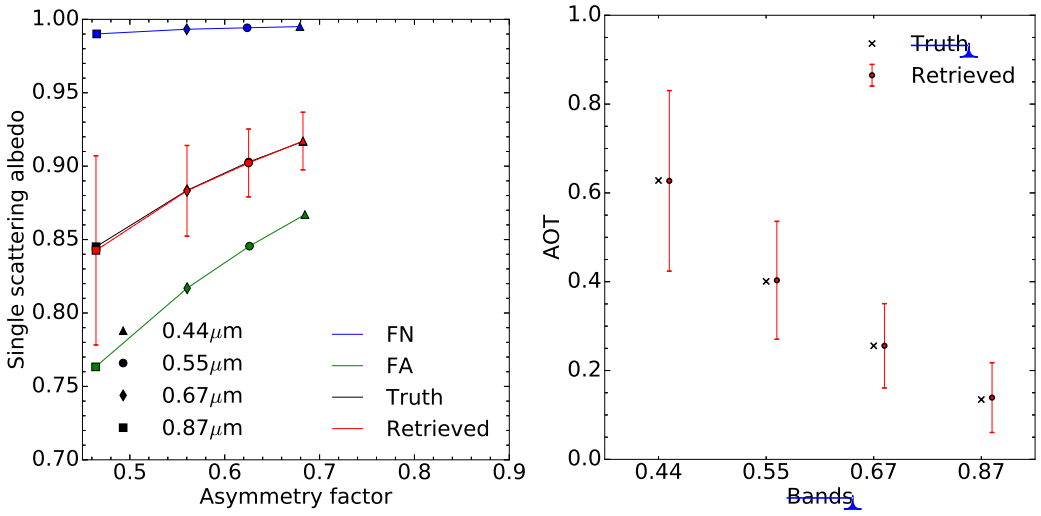

Fig. 5. Left panel: Results of experiment F00 in the $[g,\omega_0]$ space. The aerosol vertices used for the inversion are FN (blue) and FA (green). The forward aerosol properties are shown in black and the retrieved ones in red. Vertical and horizontal red bars indicate the uncertainty~~, if any,~~ of the retrieved values. **Right panel**: Retrieved AOT ~~in the four processed spectral bands~~ (red circles). The retrieval uncertainty is shown with the vertical red lines. True values are indicated with black crosses.

6.2 Results

6.2.1 Experiment F00

The purpose of the first experiment (F00) is to demonstrate that the CISAR algorithm can accurately retrieve aerosol properties in a simple situation, showing therefore that the inversion process works correctly. The F0 aerosol class used to simulate the observations is only composed of fine particles with a median radius of 0.08μm, *i.e.*, the same value as for the FN and FA vertices used for the inversion. Hence, ~~only~~ the imaginary part of the index of refraction ~~differs from the values used for the generation of these two vertices~~, the real part being set to 1.4. With ~~such~~ a retrieval configuration restricted to ~~the use of~~ only two vertices, the solution space for each wavelength is limited to a straight line between the two vertices.

Results are shown in Fig. (5) for the atmosphere and Table (6) for the surface. The asymmetry factor g and single scattering albedo ω_0 are almost exactly retrieved. There is practically no uncertainty in the retrieval of g because of the constraints imposed by the fact that the particle radius is the same as for the F0 aerosol class. The estimated single scattering albedo uncertainty is much larger ~~than the asymmetry one~~, though the retrieved values match ~~exactly~~ the true ones. The retrieved AOT is also in very good agreement with the true values as can be seen on the right panel ~~in Fig. (5)~~. ~~To further evaluate the performance of the CISAR algorithm, the~~ retrieval error ϵ_τ is defined as the difference between the retrieved and the true AOT values. Results are summarised in Table (7). This

first experiment demonstrates that it is possible to retrieve the properties of the aerosol class F0 as a linear combination of the vertices FA and FN when only the absorption varies, the particle median radius being constant.

A comparison between Tables (5) and (6) shows that the surface parameters are very accurately retrieved. As stated in Section (6.1), prior information on the magnitude of the RPV parameter is assumed unbiased with an uncertainty of 0.03. The corresponding posterior uncertainties exhibit a significant decrease for the ρ_0 parameter at all wavelengths. A similar behaviour is not observed for the other parameters. As explained in Wagner et al. (2010), the k and Θ parameters, controlling the surface reflectance anisotropy, are strongly correlated with amount atmospheric scattering. Consequently, the retrieved uncertainties decrease with ~~the~~ wavelengths, *i.e.*, as a function of the actual AOT. Despite the observations are taking place in the principal plane, the posterior uncertainty on the hot spot parameter remains equal to the prior one as a result of atmospheric scattering. This fact is attributed to the relatively high value of the true AOT, and the consequent amount of scattering ~~able to attenuate~~ the hot spot ~~effects~~. Results for the surface parameter retrieval exhibits a very similar behaviour for the other experiments and will not be shown.

Table 6. Values of the retrieved surface RPV parameters and associated uncertainties for experiment F00. Wavelengths are given in μm.

	Value				Uncertainty			
Band	ρ_0	k	Θ	ρ_c	ρ_0	k	Θ	ρ_c
	Posterior							
0.44	0.025	0.666	-0.150	0.125	0.006	0.030	0.030	0.030
0.55	0.047	0.657	-0.116	0.023	0.004	0.029	0.028	0.030
0.67	0.056	0.711	-0.096	0.025	0.004	0.028	0.026	0.030
0.87	0.238	0.705	-0.020	0.029	0.011	0.025	0.017	0.030

6.2.2 Experiment F10

Let us now examine the case where both ~~the~~ r_m and n_i ~~used to describe the forward aerosol properties~~ differ from those of the vertices used for the inversion. ~~For that purpose, aerosol~~ type F1 is used for the forward simulation with $r_{mf} = 0.1\mu$m for the predominant fine mode and $r_{mc} = 0.93\mu$m for the coarse mode. The same aerosol vertices as in experiments F00 are used for the inversion.

The results in Fig. (6) show that ω_0 is reasonably well retrieved unlike the g parameter, which is systematically underestimated. At any given wavelengths, it is not possible to retrieve g values outside the bounds defined by the FA and FN vertices. Consequently, the retrieved AOT values are underestimated by about 10% (Table 7). Additionally, the estimated error on g is largely underestimated. This example illustrates the retrieval failure when the actual solution lays outside the $[g,\omega_0]$ space defined by the active vertices.

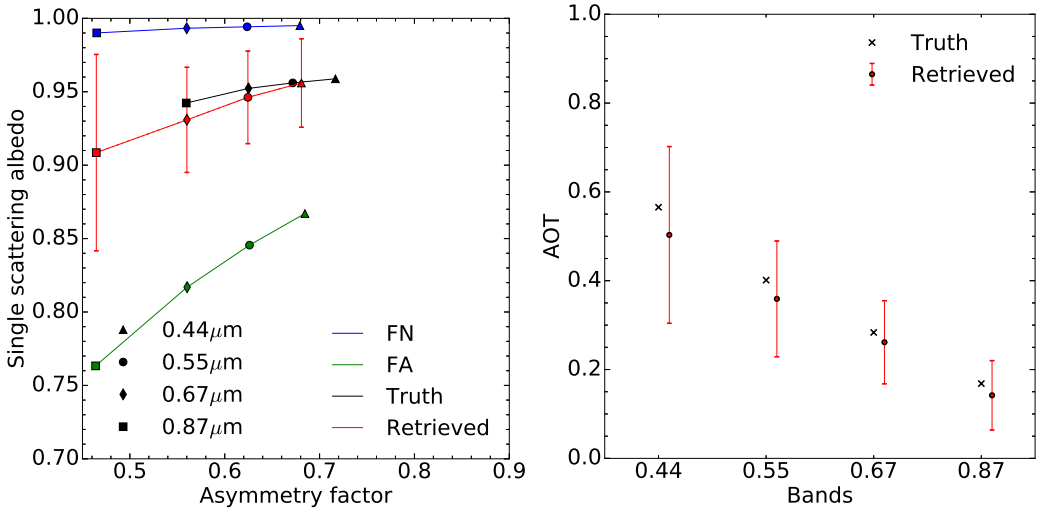

Fig. 6. Same as Fig. (5) but for experiment F10.

Table 7. Retrieved AOT error and uncertainties for the six experiments ~~in the four processed bands~~. The ~~ϵ_τ symbol is the~~ error calculated as the difference between the retrieved ~~value and the truth~~, δ_τ the relative error in percent and σ_τ the retrieval uncertainty estimated with Equation (21).

BAND	0.44			0.55			0.67			0.87		
EXP	ϵ_τ	δ_τ (%)	σ_τ	ϵ_τ	δ_τ (%)	σ_τ	ϵ_τ	δ_τ (%)	σ_τ	ϵ_τ	δ_τ (%)	σ_τ
F00	0.001	-0.1	0.203	-0.002	0.6	0.133	-0.000	0.0	0.095	-0.004	3.3	0.079
F10	0.062	-11.0	0.199	0.042	-10.5	0.130	0.022	-7.8	0.094	0.026	-15.6	0.078
F11	0.005	-0.9	0.239	-0.021	5.3	0.164	-0.037	13.2	0.125	-0.047	27.8	0.095
F12	0.041	-7.3	0.228	0.013	-3.3	0.152	-0.004	1.5	0.113	-0.015	8.6	0.089
F13	-0.001	0.1	0.295	-0.028	6.9	0.199	-0.041	14.5	0.145	-0.051	30.5	0.103
F21	0.018	-3.9	0.252	0.037	-9.2	0.172	0.042	-11.9	0.129	0.071	-22.9	0.096
F22	-0.018	3.9	0.236	-0.007	1.8	0.158	-0.004	1.1	0.116	0.008	-2.6	0.090
F23	-0.041	8.8	0.296	-0.031	7.8	0.200	-0.027	7.5	0.145	-0.018	6.0	0.103

6.2.3 Experiments F11 - F13

In order to improve the retrieval of the F1 aerosol class properties, the additional aerosol CS vertex ~~has been~~ added in layer L_a during the inversion process~~, *i.e.*, a coarse mode with $r_m = 0.3\mu$m.~~ Results of experiment F11 are displayed ~~on~~ Fig. (7). Retrieved g values are no longer ~~systematically~~ underestimated. The single scattering albedo is slightly underestimated. It should be noted that the estimated uncertainty associated with g increases with wavelength and is particularly large at 0.87μm, but rather underestimated at 0.44μm. The improvement in the AOT retrieval accuracy is noticeable in the 0.44μm and 0.55μm bands where the magnitude of ϵ_r is reduced from 0.062 to

0.005 and from 0.042 to -0.021 respectively (Table 7). At larger wavelengths, the benefit of adding the CS vertex is less noticeable though the magnitude of ϵ_r remains below 0.05. Finally, the retrieval uncertainty slightly increases from 0.199 up to 0.239 ~~in~~ the 0.44μm band because of the use of additional state variables τ_v associated with the inclusion of an additional vertex.

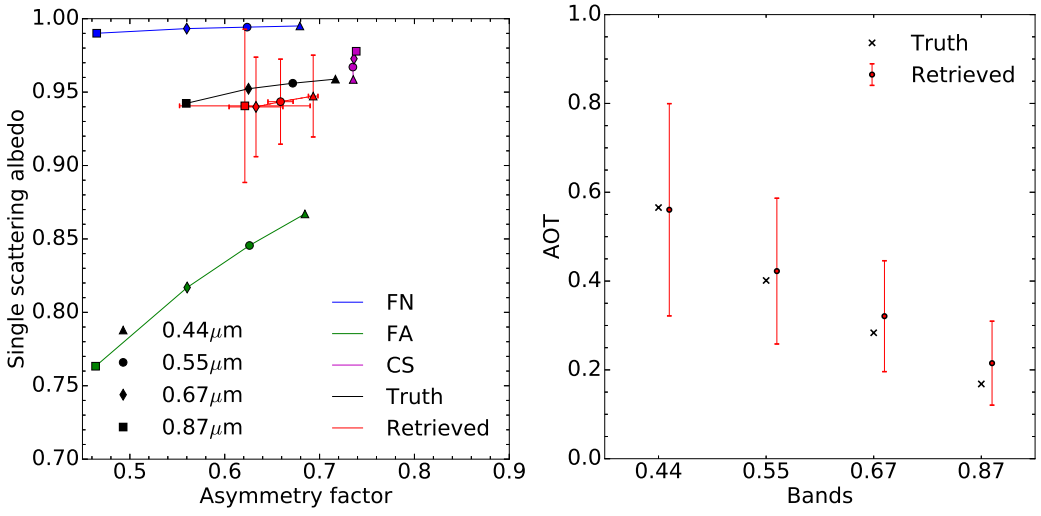

Fig. 7. Same as Fig. (5) but for experiment F11.

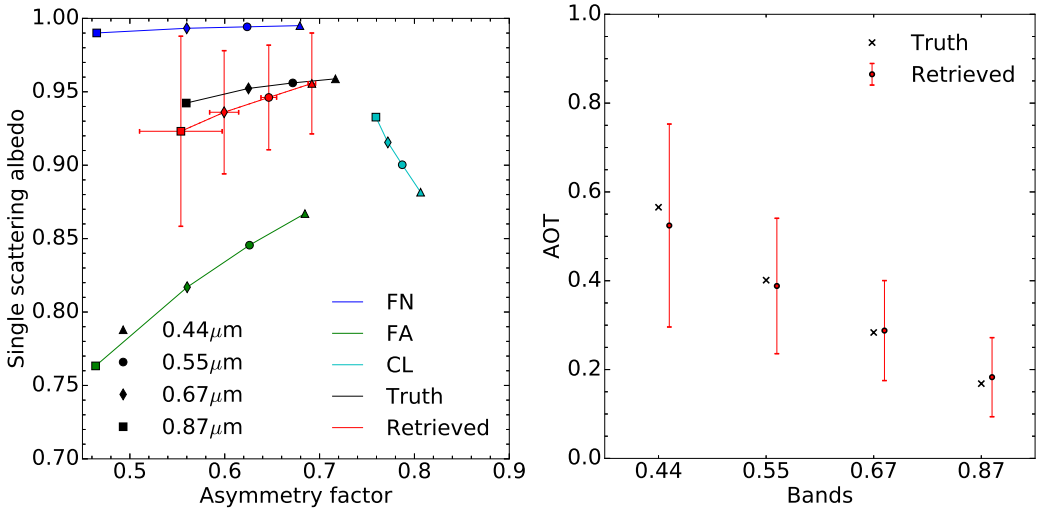

Fig. 8. Same as Fig. (5) but for experiment F12.

For experiment F12, the CS vertex is substituted by vertex CL which has a median radius of 1.0μm. The use of this vertex instead of CS considerably improves the retrieval of g and of ω_0 at large wavelengths (Fig. 8). As can be seen in Fig. (2), the sensitivity of aerosol single scattering properties to particle median radius and imaginary part of the refractive index depends on the wavelength.

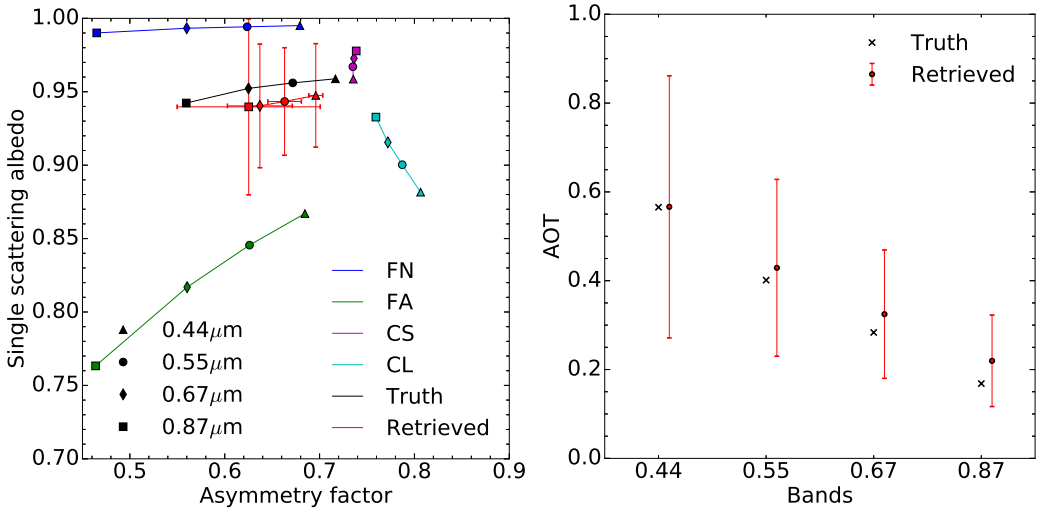

Fig. 9. Same as Fig. (5) but for experiment F13.

Hence, a similar behaviour of the algorithm ~~in~~ all wavelengths should not be expected. The errors ϵ_τ in this experiment ~~F12~~ are further reduced compared to experiment F11 with the exception of the 0.44μm band. The CISAR algorithm manages to correctly retrieve the total AOT.

Finally, the inversion ~~has been~~ performed using all four vertices (Fig. 9) ~~in experiment F13~~. This additional degree of freedom translates into an increase of the estimated uncertainty $\sigma_{\hat{\tau}}$ as a result of the large number of possible way to combine these four vertices to retrieve the properties of the aerosol class F1. In other words, adding two coarse mode vertices does not improve the characterization of F1. The actual benefit of adding this fourth vertex is therefore not straightforward, and should be noted that increasing the number of vertices impacts the computational time. This series of ~~simple three~~ experiments has shown that the use of the FN, FA and CL vertices provides the best combination for the retrieval of the properties of aerosol class F1. With this combination, the FN and FA vertices allow to control the amount of radiation absorbed by the aerosols and the CL vertex the effects of the particle size.

6.2.4 Experiments F21 - F23

The retrieval of aerosol class F2, a dual-mode particle size distribution dominated by coarse particles, is now examined. This class is composed of a fine mode radius r_{mf} ~~of~~ 0.08μm and coarse mode ~~one~~ r_{mc} ~~of~~ 0.77μm. As for the retrieval of the F1 aerosol class, three combinations of vertices have been explored, *i.e.*, (FN, FA, CS) for experiment F21 (Fig. 10), (FN, FA, CL) for experiment F23 (Fig. 11) and ~~finally~~ (FN, FA, CS, CL) for experiment F22 (Fig. 11). Essentially the same conclusions hold as for the retrieval of aerosol class F1. The retrieval of F2-class properties expressed as a linear combination of the (FN, FA, CL) vertices provides the best solution~~. Values of~~ both g and ω_0 ~~are~~ well retrieved at all wavelengths.

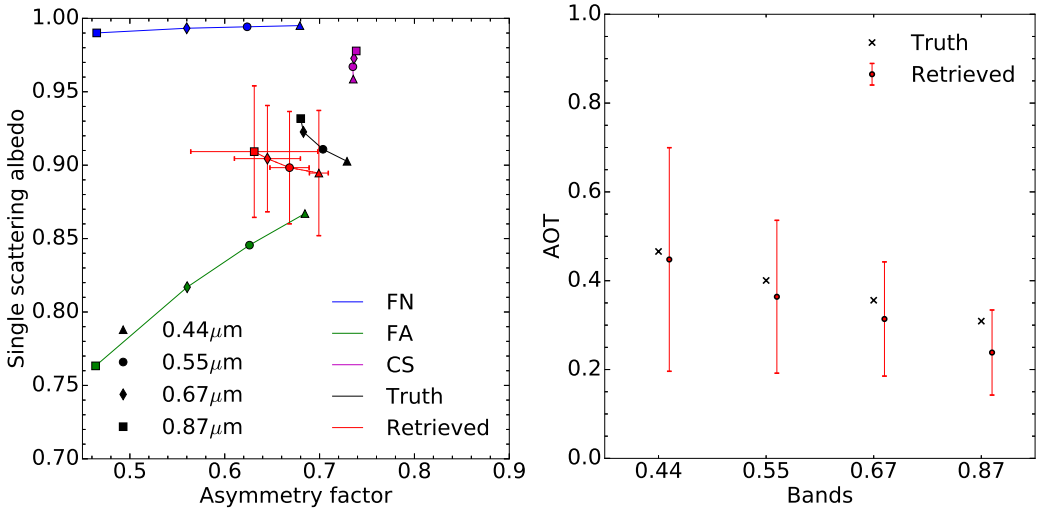

Fig. 10. Same as Fig. (5) but for experiment F21.

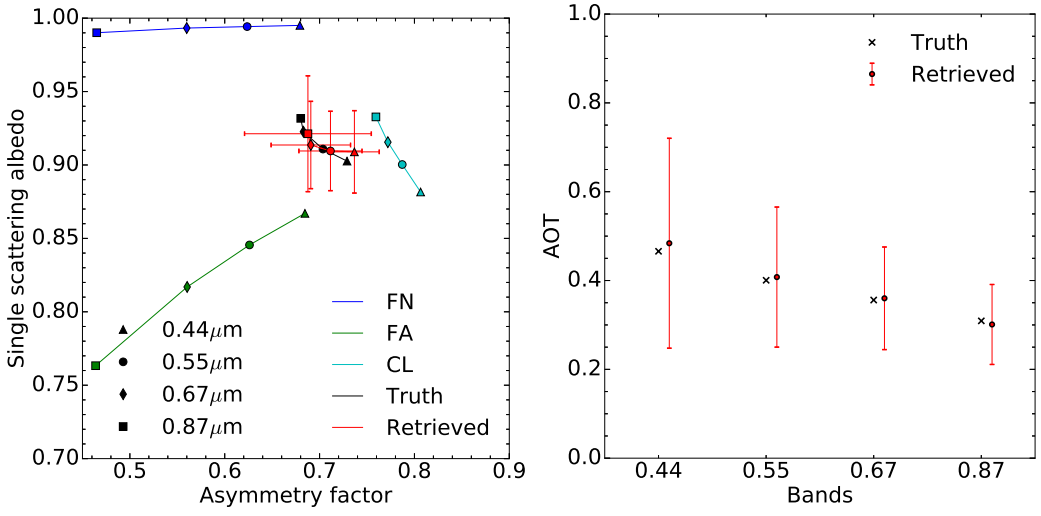

Fig. 11. Same as Fig. (5) but for experiment F22.

7 Discussion and conclusion

This paper describes the CISAR algorithm designed for the joint retrieval of surface reflectance and aerosol properties. Previous attempts to perform such joint retrieval have been reviewed, discussing their advantages and weaknesses. ~~That analysis revealed that retrieval~~ methods based on OE applied only to a limited number of aerosol classes represent a major drawback as it does not permit a continuous variation of the state variables in the solution space. The new method presented in this paper specifically addresses this issue, allowing continuous variations of the aerosol single scattering properties in the solution space without ~~having~~ the aerosol micro-physical properties explicitly appearing

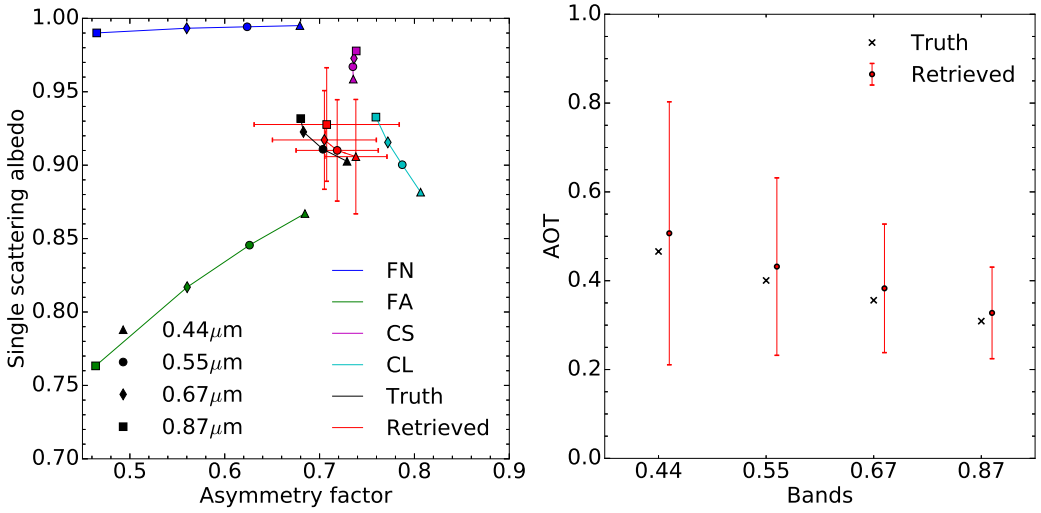

Fig. 12. Same as Fig. (5) but for experiment F23.

as state variables.

A fast forward radiative transfer model has been designed ~~for this purpose~~, which solves the radiative transfer equation without relying on pre-computed look-up tables. This model considers ~~only~~ two layers ~~in the atmosphere~~. The upper layer only hosts molecular absorption. The lower layer accounts for both absorption and scattering processes due to aerosols and molecules and is radiative coupled with the surface represented with the RPV BRF model. Single scattering aerosol properties in this layer are expressed as a linear combination of the properties of vertices enclosing the solution space.

A series of different experiments has been devised to analyse the behaviour of the CISAR algorithm and its capability to retrieve aerosol single scattering properties as well as optical thickness. This discussion focuses on the retrieval of aerosol classes ~~F1~~ dominated by the fine mode ~~and F2 dominated~~ by ~~the~~ coarse mode. These two classes have pretty different spectral behaviour in the $[g,\omega_0]$ space and yet the CISAR algorithm is capable of retrieving the corresponding single scattering properties in both cases.

These experiments illustrate the possibility to use Equations (8) and (9) for the continuous retrieval of the aerosol single scattering albedo and ~~phase function properties in the solution space.~~ These equations assume a linear behaviour of ω_0 and g in the solution space ~~illustrated in Fig. (3) as a function of the variations of the aerosol micro physical properties~~. Such assumptions have proven to be valid for the case addressed in experiment F00. This assumption is not exactly true for the retrieval of more realistic aerosol classes composed of a fine and a coarse participle size modes. However, the retrieved aerosol single scattering properties are derived much more accurately than with a method based on a limited number of predefined aerosol classes as in Govaerts et al. (2010) where ~~only~~ the single scattering properties of ~~the~~ predefined classes ~~can be exactly~~ retrieved. It thus

represents a major improvement with respect to these type of retrieval approaches without requiring the use of a large number of state variables as in the method proposed by Dubovik et al. (2011), where aerosol micro-physical properties are explicitly included in the set of retrieved state variables.

The choice of the vertices outlining the $[g,\omega_0]$ solution space is critical. In these experiments, best retrieval is obtained using three vertices, *i.e.*, one vertex composed of small weakly absorbing particles (FN), one vertex composed of small absorbing particles (FA) and one vertex composed of large particles (CL). The use of a fourth vertex (CS) does not improve the retrieval and increases the estimated retrieval uncertainty.

This set of experiments represents ideal conditions, *i.e.*, noise-free observations in the principal plane with no bias on the surface prior. This choice is motivated by the need to keep the result interpretation simple, the primary objective being to illustrate how the new retrieval concept developed in this paper works. These experiments show the possibility to retrieve aerosol single scattering properties within the solution space provided it is correctly bounded by the vertices. It is clear that adding noise in the observations will degrade the quality of the retrieval. Similar conclusions can hold in case the observations are taking place far from the principal plane where most of the angular variations occur. It should be stressed that this approach can also be applied for the retrieval of similar properties within a single cloud layer or a mixture of cloud and aerosol.

Such an algorithm therefore represents a decisive improvement with respect to the method proposed by Govaerts et al. (2010) which retrieves the aerosol optical thickness only for the very limited number of pre-defined aerosol classes. The CISAR algorithm allows a continuous variation of the aerosol single scattering properties adding only a limited number of state variables, *i.e.*, the optical thickness of each vertices.

8 Acknowledgements

Acknowledgements. The authors would like to thanks the reviewers for their fruitful suggestions.

References

Cox, C. and Munk, W.: Measurement of the Roughness of the Sea Surface from Photographs of the Sun's Glitter, Journal of the Optical Society of America, 44, 838–850, doi:10.1364/JOSA.44.000838, 1954.

Diner, D. J., Hodos, R. A., Davis, A. B., Garay, M. J., Martonchik, J. V., Sanghavi, S. V., von Allmen, P., Kokhanovsky, A. A., and Zhai, P.: An optimization approach for aerosol retrievals using simulated MISR radiances, Atmospheric Research, 116, 1–14, doi:10.1016/j.atmosres.2011.05.020, 2012.

Dubovik, O., Sinyuk, A., Lapyonok, T., Holben, B. N., Mishchenko, M., Yang, P., Eck, T. F., Volten, H., Munoz, O., Veihelmann, B., van der Zande, W. J., Leon, J. F., Sorokin, M., and Slutsker, I.: Application of spheroid models to account for aerosol particle nonsphericity in remote sensing of desert dust, Journal of Geophysical Research-Atmospheres, 111, 11 208–11 208, 2006.

Dubovik, O., Herman, M., Holdak, A., Lapyonok, T., Tanr, D., Deuz, J. L., Ducos, F., Sinyuk, A., and Lopatin, A.: Statistically optimized inversion algorithm for enhanced retrieval of aerosol properties from spectral multi-angle polarimetric satellite observations, Atmospheric Measurement Techniques, 4, 975–1018, 2011.

Fischer, J. and Grassl, H.: Radiative transfer in an atmosphere-ocean system: an azimuthally dependent matrix-operator approach, Applied Optics, 23, 1032–1039, 1984.

Govaerts, Y. and Lattanzio, A.: Retrieval Error Estimation of Surface Albedo Derived from Geostationary Large Band Satellite Observations: Application to Meteosat-2 and -7 Data, Journal of Geophysical Research, 112, doi:10.1029/2006JD007 313, 2007.

Govaerts, Y., Luffarelli, M., and Damman, A.: Effects of Sky Radiation on Surface Reflectance: Implications on The Derivation of LER from BRF for the Processing of Sentinel-4 Observations, in: Living Planet Symposium 2016, Prague, Czech Republic, Prague, Czech Republic, 2016.

Govaerts, Y. M.: RTMOM V0B.10 User's Manual, 2006.

Govaerts, Y. M., Lattanzio, A., Taberner, M., and Pinty, B.: Generating global surface albedo products from multiple geostationary satellites, Remote Sensing of Environment, 112, 2804–2816, doi:10.1016/j.rse.2008.01.012, http://www.sciencedirect.com/science/article/pii/S0034425708000412, 2008.

Govaerts, Y. M., Wagner, S., Lattanzio, A., and Watts, P.: Joint retrieval of surface reflectance and aerosol optical depth from MSG/SEVIRI observations with an optimal estimation approach: 1. Theory, Journal of Geophysical Research, 115, doi:10.1029/2009JD011 779, 2010.

Hess, M., Koepke, P., and Schult, I.: Optical properties of aerosols and clouds: The software package OPAC, Bulletin of the American Meteorological Society, 79, 831–844, 1998.

Kokhanovsky, A. A., Deuz, J. L., Diner, D. J., Dubovik, O., Ducos, F., Emde, C., Garay, M. J., Grainger, R. G., Heckel, A., Herman, M., Katsev, I. L., Keller, J., Levy, R., North, P. R. J., Prikhach, A. S., Rozanov, V. V., Sayer, A. M., Ota, Y., Tanr, D., Thomas, G. E., and Zege, E. P.: The inter-comparison of major satellite aerosol retrieval algorithms using simulated intensity and polarization characteristics of reflected light, Atmos. Meas. Tech., 3, 909–932, doi:10.5194/amt-3-909-2010, 2010.

Lattanzio, A., Schulz, J., Matthews, J., Okuyama, A., Theodore, B., Bates, J. J., Knapp, K. R., Kosaka, Y., and Schller, L.: Land Surface Albedo from Geostationary Satelites: A Multiagency Collaboration within SCOPE-CM, Bulletin of the American Meteorological Society, 94, 205–214, doi:10.1175/BAMS-D-11-00230.1, 2013.

Liu, Q. and Ruprecht, E.: Radiative transfer model: matrix operator method, Applied Optics, 35, 4229–4237,

1996.

Luffarelli, M., Govaerts, Y., and Damman, A.: Assessing hourly aerosol properties retrieval from MSG/SEVIRI observations in the framework of aeroosl-cci2, in: Living Planet Symposium 2016, Prague, Czech Republic, Prague, Czech Republic, 2016.

Luffarelli, M., Govaerts, Y., Goossens, C., Wolters, E., and Swinnen, E.: Joint retrieval of surface reflectance and aerosol properties from PROBA-V observations, part I: algorithm performance evaluation, in: Proceedings of MultiTemp 2017, Bruges, Belgium, 2017.

Manolis, I., Grabarnik, S., Caron, J., Bzy, J.-L., Loiselet, M., Betto, M., Barr, H., Mason, G., and Meynart, R.: The MetOp second generation 3MI instrument, p. 88890J, doi:10.1117/12.2028662, 2013.

Marquardt, D.: An Algorithm for Least-Squares Estimation of Nonlinear Parameters, SIAM Journal on Applied Mathematics, 11, 431–441, 1963.

Pinty, B., Roveda, F., Verstraete, M. M., Gobron, N., Govaerts, Y., Martonchik, J. V., Diner, D. J., and Kahn, R. A.: Surface albedo retrieval from Meteosat: Part 1: Theory, Journal of Geophysical Research, 105, 18 099–18 112, 2000a.

Pinty, B., Roveda, F., Verstraete, M. M., Gobron, N., Govaerts, Y., Martonchik, J. V., Diner, D. J., and Kahn, R. A.: Surface albedo retrieval from Meteosat: Part 2: Applications, Journal of Geophysical Research, 105, 18 113–18 134, 2000b.

Rahman, H., Pinty, B., and Verstraete, M. M.: Coupled surface-atmosphere reflectance (CSAR) model. 2. Semiempirical surface model usable with NOAA Advanced Very High Resolution Radiometer Data, Journal of Geophysical Research, 98, 20,791–20,801, 1993.

Rodgers, C. D.: Inverse methods for atmospheric sounding, Series on Atmospheric Oceanic and Planetary Physics, World Scientific, 2000.

Schuster, G. L., Dubovik, O., Holben, B. N., and Clothiaux, E. E.: Inferring black carbon content and specific absorption from Aerosol Robotic Network (AERONET) aerosol retrievals, Journal of Geophysical Research, 110, S1017–S1017, 2005.

Serene, F. and Corcoral, N.: PARASOL and CALIPSO : Experience Feedback on Operations of Micro and Small Satellites, in: SpaceOps 2006 Conference, American Institute of Aeronautics and Astronautics, dOI: 10.2514/6.2006-5919, 2006.

Vermote, E. F., Tanré, D., Deuzé, J. L., Herman, M., and Morcrette, J. J.: Second simulation of the satellite signal in the solar spectrum, 6S: An overview, IEEE TGARS, 35, 675–686, 1997.

Wagner, S. C., Govaerts, Y. M., and Lattanzio, A.: Joint retrieval of surface reflectance and aerosol optical depth from MSG/SEVIRI observations with an optimal estimation approach: 2. Implementation and evaluation, Journal of Geophysical Research, 115, doi:10.1029/2009JD011 780, 2010.

Wiscombe, W. J.: The Delta-M Method: Rapid Yet Accurate Radiative Flux Calculations for Strongly Asymmetric Phase Functions, Journal of Atmospheric Sciences, 34, 1408–1422, 1977.

REVIEW OF 'JOINT RETRIEVAL OF SURFACE REFLECTANCE AND AEROSOL PROPERTIES WITH CONTINUOUS VARIATIONS OF THE STATE VARIABLES IN THE SOLUTION SPACE: PART 1: THEORETICAL CONCEPT'

This paper outlines an algorithm to retrieve surface reflectance and optical properties of atmospheric aerosol from visible and infrared satellite imagery. The vast majority of equivalent algorithms (including previous iterations of this technique) assume the optical properties of the aerosol particles observed (known as the aerosol type). The paper proposes considering multiple types simultaneously, such that the retrieval can freely explore a continuous space in single scattering albedo and asymmetry factor. A theoretical demonstration of the algorithm is presented using idealised data.

I wish to clearly state that I quite like the idea behind this algorithm. Single-scattering albedo and the asymmetry parameter provide a theoretically superior state space in which to evaluate aerosol retrievals and I would love to see (and do) more research around this idea. I am always pleased to see a discussion of information theory in an atmospheric science paper and more validation papers should discuss uncertainty. I want to see this pair of papers eventually published.

My issue is that I see no evidence that this algorithm currently produces acceptable results. Even in the idealised circumstances presented here, the retrieval exhibits biases in AOD of up to 0.04 and the reported uncertainties of 0.1 - 0.3 are well in excess of any method I'm familiar with. Even looking in the SSA-g space used by most of the figures, the uncertainty on each term is substantial. For example, the 440 µm point in Fig. 11 occupies about a third of the area defined by Fig. 3. I know retrieving SSA is difficult, and the uncertainties should therefore be large, but the tone of this paper is entirely unjustified by the results presented. The introduction and conclusions need to be toned down to represent the quality of the results.

The revisions to the manuscript are an improvement, but the authors seem to have disagreed with the majority of my original comments. My apologies for being unclear — I shall try again. I leave it to the discretion of the editor which, if any, of the following should be addressed in a further revision.

- I still think you should have applied the retrieval to noisy data. I'm not asking for a perfect satellite simulation that replicates real viewing conditions and different spectral response function. Merely adding 3 % random perturbations to the observations underlying experiment F12 and F22 would be sufficient. There needs to be some evidence that the algorithm can deal with unavoidable noise to be of practical use. Such an analysis might also demonstrate that your predicted uncertainties are justified, improving the reader's confidence in your technique. (I'd actually prefer to see a thorough sensitivity study of bias as a function of the various parameters rather than the simple 1 - 3 % uncertainty you've added, but that can be in a third paper.)

- I remain unhappy that a joint retrieval of aerosol and the surface is promised but only aerosol is discussed. There's a hint of a quite good surface retrieval at the end of Part 2 (and it's supplement). Yes, this paper is describing how the aerosol retrieval has been improved but your previous paper was from 2010. You can't have left the surface retrieval completely unaltered over almost a decade of research and, even if you did, I'd be rather surprised if all the changes you made to the aerosol scheme didn't impact the response of the surface scheme in some way. As you point out in your first sentence, the two are non-linearly coupled. Why decouple the papers when there's only one forward model?

- On L118, I don't think LUTs should be mentioned. The problems your describe aren't caused by the use of LUTs, but rather the use of LUTs that are either too coarse or are tabulated for insufficiently general variables. It is possible to build LUTs that have SSA and g as their axes. (As a side note, the GRASP algorithm of Dubovik's group was demonstrated on PARASOL data but can be, and has been, adapted to any sensor. As the information content decreases, the reliance on the prior increases.)

- You're entitled to use whatever terminology you like, but why not call the terms 'surface' and 'atmosphere' as you did in Govaerts et al. (2010)? 'Single' scattering could describe both single scattering by the surface and single scattering by an aerosol.

- You missed my point about the beginning of your conclusions (now L425) for the example I gave. The third sentence of the conclusions implies you provided evidence of a fundamental flaw in retrievals that assume an aerosol type. You did no such thing and this statement should either be removed or edited to be accurately represented as an opinion.

- Apologies for my unclear remark on the title. Throughout the paper, you argue that assuming aerosol type is inconsistent with the assumptions of OE. I agree with that technical point. It is conceptually preferable to define state space in terms of the microphysical properties, as you have done. However, 'continuous variations of the state variables in solution space' will not convey that point to most readers as 'state variables' is not specific and all OE involves continuous variation of variables. Your enhancement is to select different variables to retrieve and constrain them through a choice of aerosol type (a.k.a. vertices).

  Your paper proposes something between Dubovik's direct retrieval of SSA-phase function and the assumed type of your previous algorithm. Aerosol types are still assumed (presumably to get around the highly non-Gaussian nature of the SSA-g prior distribution) but the retrieval may freely combine them to produce continuous variations in SSA and g. Hence, I would recommend a title along the lines of 'Retrieval of surface reflectance and aerosol microphysical properties through the mixture of representative aerosol types' but better worded. That emphasises the variation of aerosol mixture rather than the variables themselves.

  To be pedantic, the techniques you critique are completely valid when evaluating only one type as they are effectively claiming to have perfect prior information about certain variables. That's obviously an inaccurate claim but

it's statistically consistent. The inconsistency arises from the manner in which different types are combined.

- I recommended deleting the sentence now starting on L354 as it is obvious that the uncertainty in SSA is larger than that in g since your retrieval could not vary g. As it stands, a reader unfamiliar with retrieval theory may not appreciate that your precise retrieval of g derives from having given it no other option (as the aerosol types provided demonstrate no variation in g.)

A few more comments that occurred during my most recent read of the work,

- Reading through Part 2, it became evident that Part 1 demonstrates retrievals using only one observation while Part 2 combines observations from 5-16 days. Why didn't you demonstrate the retrieval you actually intend to use? Presumably the additional data would improve the retrieval and provide better agreement? You spent several pages introducing the **H** matrices but it doesn't seem they played that much of a role in this paper. And, anticipating your response, a reader will be no more distracted by a few additional plots than they already are by Figs. 6-12. The retrievals could be plotted on the same axes, hopefully showing a reduction in uncertainty and bias as more overpasses are included.

- If not doing that, I agree with the other reviewer's comments that Fig. 6-9 and 10-12 could be merged into single figures to facilitate comparison of the retrievals as a function of the vertices used.

L18 I'd prefer to say "can be modelled as" rather than "is equivalent to" as there are various possible models for this particular problem.

L309 Could you be more specific than 'small' about this threshold?

L379 I disagree that ω_0 is well retrieved; at 870 nm it's off by 0.03. The retrieved values are *consistent* with the truth, but so is half of the available range. If you insist that getting the range right is noteworthy, you need to provide an idea of how good these sorts of retrievals normally are and my memory is that AERONET is more accurate than 0.03 in these conditions. If I remember incorrectly, my apologies.

L382 This uncertainty isn't underestimated — it is merely wrong. The retrieval wasn't given the ability to change g and so it considers it's retrieval to be very accurate.

- In the conclusions, it would be more honest to mention the significant uncertainties in your retrievals at the end of L444 and to remove the word 'major' on L454.

And some grammatical recommendations,

L21 the amount of sky incident radiation

L33 improve to allow permit the processing

L71 Finally, the possibility ability to

L127 be applied on to the entire

L172 similar approach as to the one

L182 way. In the case of When processing of actual satellite data

L254 often assumed being to be acquired

L255 Such a situation

Eq.11 Plus signs are missing between the terms.

L355 retrieved values match exactly exactly match the true

L367 correlated with the amount of atmospheric

L369 the observations are taking place

L436 is radiatively coupled with the a surface, represented with by the RPV